Aalborg Universitet

AALBORG UNIVERSITY
DENMARK

Disordered materials for high-performance lithium-ion batteries: A review

Wang, Zhaoyang; Du, Zijuan; Wang, L.Q.; He, G.J.; Parkin, I.P.; Zhang, Y.F.; Yue, Yuanzheng

Published in:
Nano Energy

DOI (link to publication from Publisher):
10.1016/j.nanoen.2023.109250

Publication date:
2024

Document Version
Accepted author manuscript, peer reviewed version

Link to publication from Aalborg University

Citation for published version (APA):
Wang, Z., Du, Z., Wang, L. Q., He, G. J., Parkin, I. P., Zhang, Y. F., & Yue, Y. (2024). Disordered materials for high-performance lithium-ion batteries: A review. *Nano Energy*, *121*, Article 109250. https://doi.org/10.1016/j.nanoen.2023.109250

General rights
Copyright and moral rights for the publications made accessible in the public portal are retained by the authors and/or other copyright owners and it is a condition of accessing publications that users recognise and abide by the legal requirements associated with these rights.

- Users may download and print one copy of any publication from the public portal for the purpose of private study or research.
- You may not further distribute the material or use it for any profit-making activity or commercial gain
- You may freely distribute the URL identifying the publication in the public portal -

Take down policy
If you believe that this document breaches copyright please contact us at vbn@aub.aau.dk providing details, and we will remove access to the work immediately and investigate your claim.

Downloaded from vbn.aau.dk on: January 23, 2024

Disordered materials for high-performance lithium-ion batteries: a review

Zhaoyang Wang[a,1*], Zijuan Du[b,c,1], Luoqing Wang[a], Guanjie He[c], Ivan P. Parkin[c], Yanfei Zhang[d*], Yuanzheng Yue[e*]

[a] Shandong Provincial Key Laboratory of Chemical Energy Storage and Novel Cell Technology, School of Chemistry and Chemical Engineering, Liaocheng University, Liaocheng 252059, China
[b] State Key Laboratory of Silicate Materials for Architectures, Wuhan University of Technology, Wuhan 430070, China
[c] Christopher Ingold Laboratory, Department of Chemistry, University College London, London WC1H 0AJ, UK
[d] School of Materials Science and Engineering, Qilu University of Technology, Jinan 250353, China
[e] Department of Chemistry and Bioscience, Aalborg University, 9220 Aalborg, Denmark

[*]Corresponding authors: wzy9218@126.com (Z.Y. Wang), zhang-yanfei@hotmail.com (Y.F. Zhang), yy@bio.aau.dk (Y.Z. Yue)
[1] These authors contributed equally to this work.

Abstract

Disordered materials (DMs) have become promising materials in the advancement of lithium-ion batteries (LIBs). Their disordered, open structure is conductive to facilitate efficiency lithium-ion storage. DMs with tunable compositions also possess abundant defects that can interact with Li^+, further enhancing their electrochemical performances in LIBs. Yet, revealing the structural origin of the superior electrochemical properties of DM-based LIBs remains a challenge. In this article, we review recent advances in the development of DM-based components for LIBs, such as anodes, cathodes, coating layers, and solid-state electrolytes. We describe the primary preparation and characterization methods utilized for DMs, while also describing the mechanisms involved in DM synthesis. This review article also addresses the correlation between the structural properties of DMs and their electrochemical performances. Moreover, we elucidate the challenges and future perspectives in the advancement of DM-based LIBs. We summarize the key advantages of DMs in enhancing LIB performance over their crystalline counterparts, providing insights for developing superior LIBs through tailored DM development.

Keywords: Lithium-ion batteries; Disordered materials; Material preparation; Electrodes; Solid-state electrolytes; Electrochemical performances

1. Introduction

The development of sustainable and renewable energy technologies is an effective way to deal with the problems of energy crisis and climate change [1,2]. As a key step to develop such technologies, it is a necessity to advance the energy storage devices, such as the high-energy density batteries for storing green energy [3-5]. These batteries can be divided into many different categories according to the moving cations between the electrodes, such as lithium-, sodium-, magnesium-, calcium-, aluminum-, and zinc-ion batteries. To date, lithium-ion batteries (LIBs) are still the most predominant power sources in portable electronic devices since their first commercialization [6,7]. To meet the ever-increasing demand for large-scale energy applications like hybrid electric vehicles and pure electric vehicles, scientists and technologists have been continuously developing new electrode and electrolyte materials for higher energy and power densities by means of various technical routes [8,9]. Among them, the disorder strategy on both electrode and electrolyte materials for LIBs is considered to be significantly effective for the enhancement in the battery performances [10-19].

Disordered materials (DMs) differ from crystalline materials as they lack a periodic arrangement of atoms, displaying an irregular atomic structure. Disorder can manifest across different length scales, commonly categorized as short-range (< about 6 Å), medium-range (about 6-20 Å), and long-range (>20 Å) scales. DMs cover a wider range than amorphous substances. They include not only amorphous solids and liquids but also crystalline solids that contain significant defects like vacancies, interstitials, dislocations, clusters, and more. Crystalline materials can undergo complete or partial transformation into disordered solids through various disordering processes. These processes include chemical doping, impurity contamination, exposure to high-energy radiation, and ion intercalation/extraction in batteries [20]. Moreover, crystalline materials can transition into fully disordered states through mechanical impact, for instance, via high-energy ball milling. This process results in the disruption of long-range order and topological symmetry, primarily due to a substantial increase in defective surface area.

Amorphous materials, as a subset of DMs, showcase long-range disorder. They can be categorized into two groups: 1) melt-quenched glasses and 2) non-melt-quenched varieties. The differences between these two groups of materials are reflected in the following five aspects:

1) Melt-quenched glasses belong to the category of amorphous materials, but not all amorphous materials are classified as melt-quenched glasses. 2) Melt-quenched glasses result from melting raw materials and rapidly cooling the resulting melt. Conversely, non-melt-

quenched glasses can form through chemical reactions within specific temperature-pressure conditions, even at ambient levels. For instance, they are synthesized using methods like the sol-gel process and other wet-chemistry approaches. These materials, such as gel, calcium silicate hydrate phase in cement, and spin glasses, display a long-range disordered structure. Some non-melt-quenched glasses, like amorphous carbon [21,22] and disordered graphene [23], can only be synthesized under high pressure at elevated temperatures. For convenience, non-melt-quenched glasses can be referred to as amorphous materials. 3) Melt-quenched glasses undergo a calorimetric glass-liquid transition when heated, while non-melt-quenched glasses, despite lacking the X-ray Bragg diffraction patterns, do not demonstrate such a transition. 4) The key requirement for creating a melt-quenched glass is that the raw material should not decompose upon heating before reaching the melting point. The resulting liquid will undergo supercooling, quenching at a sufficiently fast rate, and eventually form glass. For instance, certain metal-organic frameworks (MOFs) can be melted before decomposing, while others tend to decompose before reaching the melting point. In the latter case, alternative methods, e.g., structural perturbation [24], are utilized to produce glasses. 5) Melt-quenched glasses can be categorized into four main families: inorganic non-metallic glasses (like oxide and chalcogenide glasses), organic glasses (such as polymer and molecular systems), metallic glasses, and MOF glasses. Notably, the structure of melt-quenched MOF glasses displays a significant degree of short-range disorder [25], differing from the other three families. The latter, while demonstrating long-range disorder, often display both medium- and short-range order within their structures.

Due to their distinct structural differences from crystalline counterparts, DMs have compelling advantages in enhancing the electrochemical properties of LIBs. First, the disordered open network structures can both effectively accommodate the mechanical stresses and volume changes upon lithiation/delithiation [26,27], and facilitate an isotropic transport of Li^+ ions [28,29]. Second, abundant defects in the structure of DM electrodes provide more reaction sites for Li^+, thereby enhancing the specific capacity of LIBs [30,31]. Third, the easy tunability of the composition and structure of DMs allows us to optimize the end-properties of LIBs [32,33]. Last but not least, DMs are less likely to undergo a phase transition during the electrochemical reactions but may experience nano-crystallization during charge/discharge cycling. The latter leads to a significant improvement in the cycling stability of LIBs [34]. Recently, the disorder-order engineering concept was proposed to enhance LIB performances [11,12]. The results showed a promising development trend of the glass-based electrodes and

electrolytes for LIBs. The mechanism of the performance enhancement of glass-based electrodes has been revealed [14-16].

This article presents a thorough overview of the applications of DMs in LIBs with an emphasis on cathodes, anodes, electrolytes, and coating layers (as illustrated in Fig. 1). We also scrutinize the synthesis methods of DMs and propose some future research directions and challenges of DMs in LIBs. We provide insight into the relationship between the structure and electrochemical properties of DMs in LIBs during cycling. This review article will benefit the rational design and property optimization of DMs for developing superior LIBs.

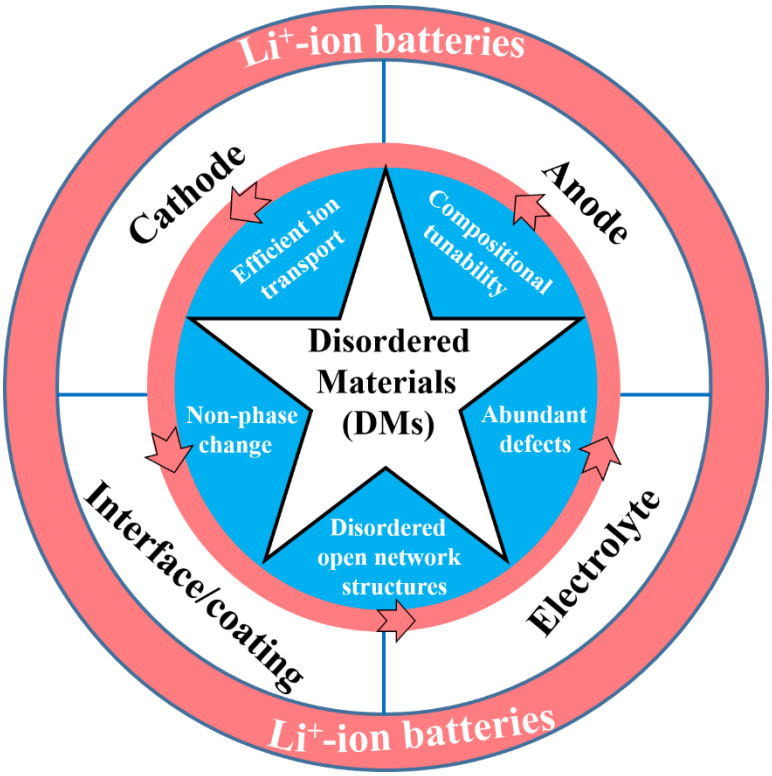

Fig. 1. Schematic of DMs' special merits, together with the functional applications of DMs in LIBs.

2. Strategies of preparation for active DMs for LIBs

The preparation methods of DMs can be generally divided into two categories according to their assembly modes, i.e., "bottom-up" and "top-down" approaches [35]. As illustrated in Fig. 2, the bottom-up approach refers to the one by which DMs are formed from the atomic level by reducing the reaction energy and/or time, such as chemical deposition, solvothermal, chemical vapor deposition (CVD) and laser deposition and electrochemical deposition [36]. In contrast, the top-down approach is the one that starts from the bulk crystal level. DMs are formed by destroying the original crystal structure

by means of melt-quenching, high-pressure, exfoliation, ball-milling, and so on [37]. These amorphization strategies are described and discussed in detail as follows.

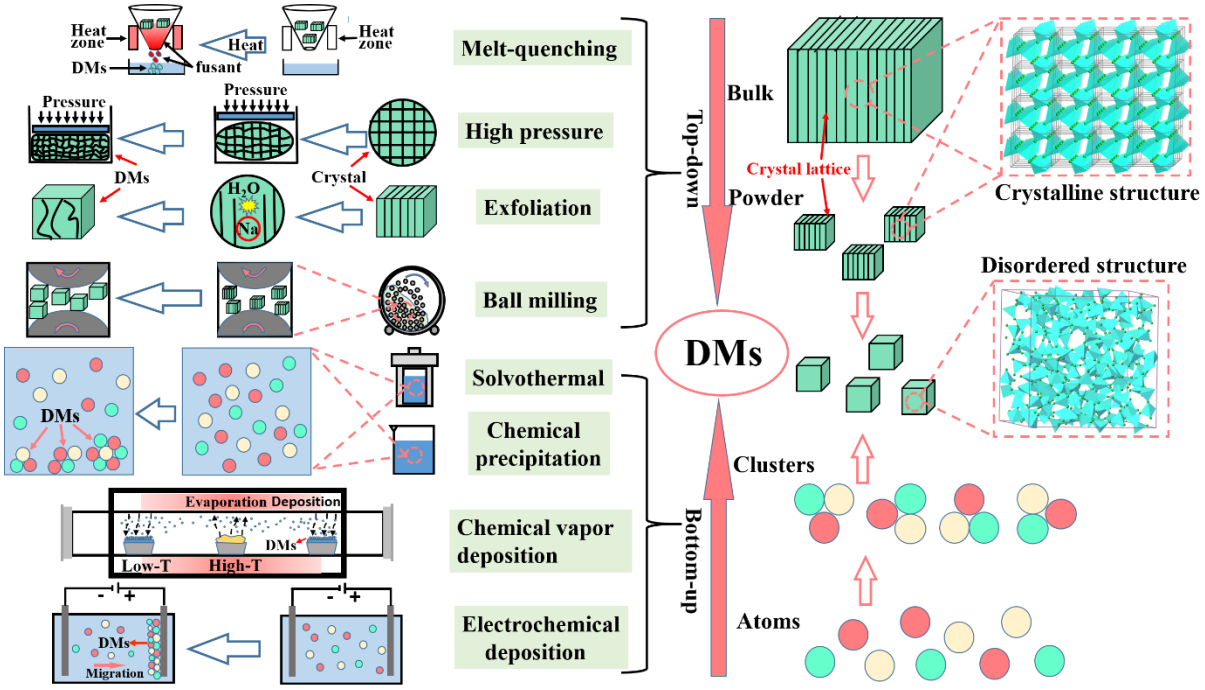

Fig. 2. Schematic illustration of DMs' synthesis strategies.

2.1 Bottom-up approach

2.1.1 Solvothermal method

It is well known that the solvothermal method is commonly used to prepare crystalline materials. The water/organic solvent can act as the reaction medium in a sealed vessel, where the pressure gradually rises with the volatilization of water/organic solvent at an elevated temperature (e.g., 200 ℃). Under such sealed conditions, the thermal energy (i.e., kinetic energy) can be increased to a level, where the energy barriers can be overcome for both formation and growth of crystals [38]. However, if the provided thermal energy is not sufficiently high to overcome the energy barrier, the formation of crystals can be avoided, but disordered intermediate products could be generated [39]. During the solvothermal reaction process, the thermal energy can be decreased by lowering the reaction temperature and/or even shortening the reaction time (Fig. 3a). For example, in the case of Ni-MOF synthesis, lowering solvothermal temperature led to the formation of large disordered clusters [40]. In addition, the solution pH can also affect the content of the disordered phase in the product [41].

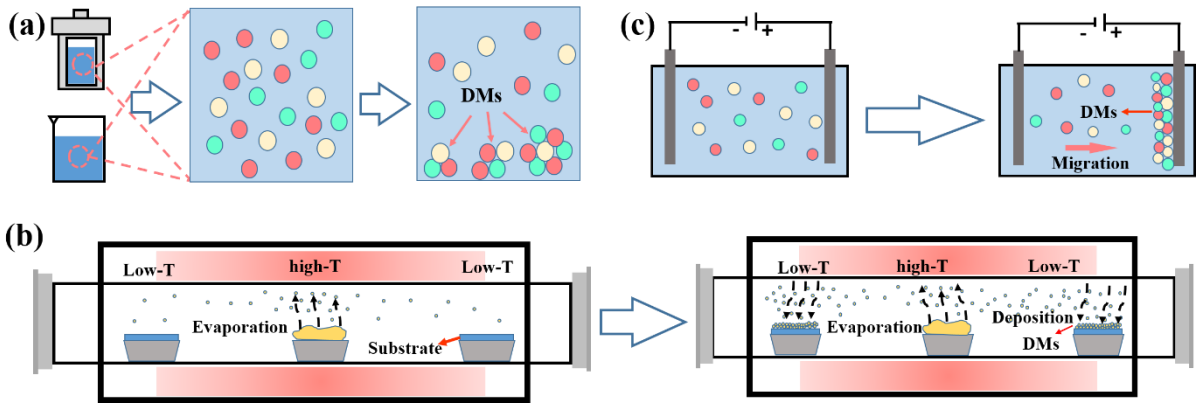

Fig. 3. Schematic illustration of the formation process of DMs by chemical precipitation method (a), CVD method (b) and electrochemical deposition method (c).

2.1.2 Chemical precipitation method

Chemical precipitation is a process in which certain agents, such as counter-ions, are added to a solution to convert some dissolved ions into insoluble compounds. To obtain disordered precipitates, some special agents such as N,N-dimethylformamide (DMF) are screened out [42]. Similar to the solvothermal method, effectively controlling the reaction time at room temperature can promote the formation of DMs (Fig. 3a) [22]. Ouyang et al. obtained disordered interconnected SiO_x-resorcinol-formaldehyde resin precipitates through a 24-hour condensation reaction at room temperature [43]. Additionally, the solubility of precipitates and the state of the end-products are affected by two key factors: 1) the reaction temperature and 2) the pH value of the solution [44]. For instance, the solubility of metal hydroxide is extremely low at low temperatures and under strong alkaline conditions. When the correct solution of metal ions is added to an alkaline solution, a disordered precipitate will form [45,46].

2.1.3 Chemical vapor deposition method

Chemical vapor deposition (CVD) is currently the most effective method for low-cost scalable preparation of two-dimensional materials. CVD is defined as the deposition of a solid material on a heated surface by a chemical reaction in the vapor phase [47]. Rapid deposition of atoms or molecules in the vapor phase occurs when they come into contact with a low-temperature (Low-T) substrate. However, due to the rapid deposition rate and low temperature, these deposited species struggle to arrange themselves into a crystal structure spontaneously, resulting in the formation of DMs (as shown in Fig. 3b). Using the CVD method, Rho et al. obtained disordered silicon films with lowered extinction coefficients compared to their crystalline counterparts [48]. Laser deposition is a special type of chemical vapor deposition method, using high-energy laser bombardment to convert the target components into a gaseous state. The resulting gases diffuse onto the surface of the substrate, subsequently forming new

films. To obtain DMs, it is necessary to lower the temperature around the substrate to reduce the thermal energy available [49].

2.1.4 Electrochemical deposition method

Electrochemical deposition is a straightforward and effective method with easily controlled process parameters for preparing DMs. As illustrated in Fig. 3c, driven by the current generated by an external circuit, the cations and anions in the electrolyte solution migrate onto the surface of the electrode to create a coating [50]. Gao et al. fabricated a three-dimensional (3D) self-supported nano-porous disordered S-doped $NiFe_2O_4/Ni_3Fe$ composite electrode via electrochemical deposition for electrocatalysis [51]. This disordered electrode exhibited higher electrocatalytic activity for oxygen evolution reaction and durability in alkaline media compared to its crystalline counterpart. Current density is a significant factor in the electrochemical deposition process [52]. Xu et al. found that the solid electrolyte interface (SEI) film is monolithic and disordered when it was prepared by the electrochemical deposition at low current densities (0.1 mA cm^{-2}). When the current density exceeded 2 mA cm^{-2}, the disordered structure of the SEI film was transformed into a crystal-embedded disordered structure [53].

2.2 Top-down approach

2.2.1 Melt-quenching method

Melt-quenching is a conventional preparation method for preparing glasses. To prevent crystallization, a liquid must be quenched at a sufficiently high rate (see Fig. 4a). The cooling rate of the melt is a vital factor for glass formation. The glass is not in a state of thermodynamic equilibrium as the liquid progresses from its supercooled state through the glass transition, ultimately reaching the glass state [54,55]. Zhang et al. prepared the V_2O_5-TeO_2 (VT) glasses using the melt-quenching method and explored the performances of the VT glass-based anodes for LIBs [11,12]. The plasma synthesis is a special type of melt-quenching method for producing a glass state, and it involves the injection of reactant powders into a hermetically sealed plasma torch. When the powders leave the plasma torch, they encounter a quenching gas and undergo rapid quenching, particularly for small-sized powers. The reactants will eventually evolve into disordered materials [56]. Westover et al. prepared the disordered $Li_{2.7}Si_{0.7}P_{0.3}O_{3.17}N_{0.22}$ electrolyte nanopowders via plasma synthesis method at a lower preparation temperature of 800 °C compared to the conventional powder sintering approach (at 1000 °C). This method can avoid the Li loss [57].

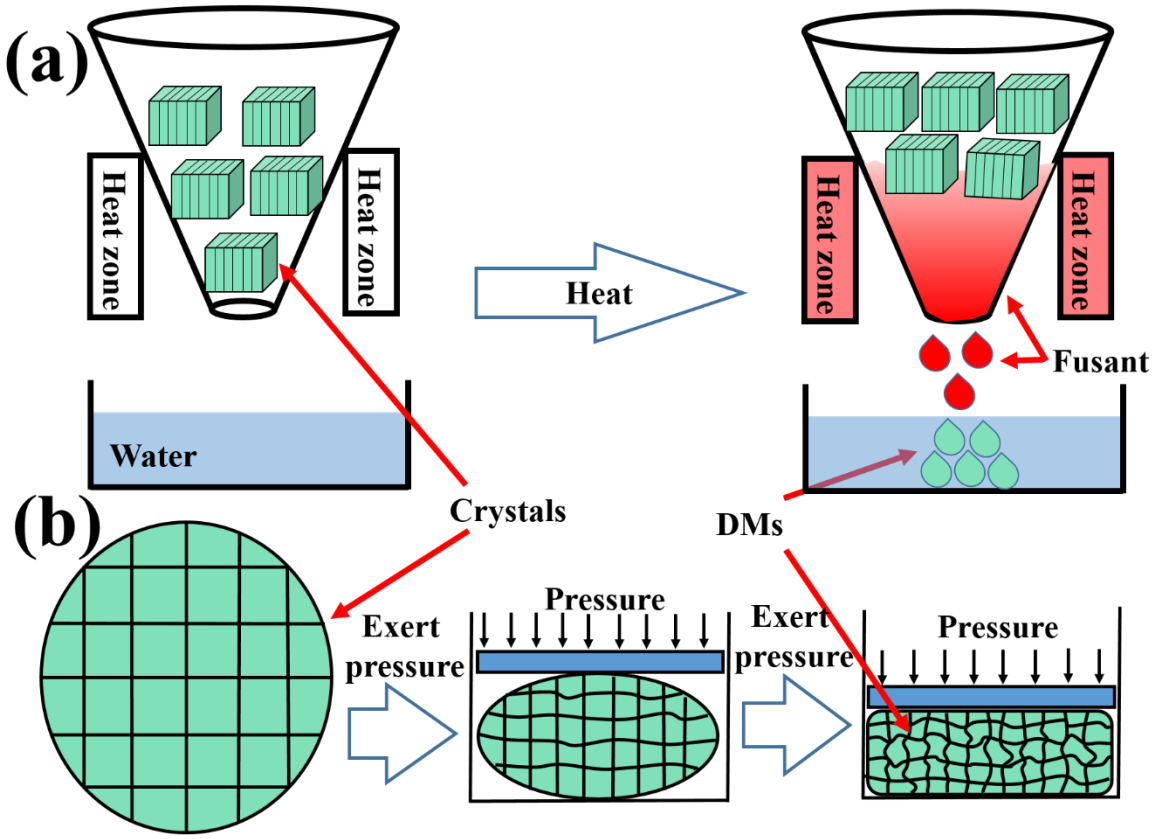

Fig. 4. Schematic illustration of the formation process of DMs by (a) melt-quenching method and (b) high-pressure method.

2.2.2 High pressure-induced amorphization method

High pressure-induced amorphization is a process whereby a crystalline material undergoes a transformation into a disordered solid by adjusting the pressure at a specific temperature. As the pressure exerted on the crystalline material gradually increases, the lattice is gradually distorted until it becomes completely disordered, forming a DM (see Fig. 4b) [22]. Wu et al. found that C_{60} crystals can become disordered due to dimerization and lattice collapse when the pressure is increased to 26.9 GPa [58]. The pressure-induced high-density phase, i.e., disordered C_{60}, played an important role in improving the energy density of LIBs when it served as an electrode material. This means that, to achieve an optimum DM for high-performance LIB, a suitable pressure should be applied during the preparation process. Wu et al. found that the cyclic stability of the $La_{0.7}Mg_{0.3}Ni_{3.3}$ alloy anode treated at 1 GPa pressure was improved by 8.7%, whereas it decreased when the pressure was increased to 3-5 GPa [59].

2.2.3 Exfoliation method

Layered crystals exhibit strong interlayer coupling and weak van der Waals bonding between layers [60]. This unique two-dimensional feature enables the layered crystals to be readily exfoliated into the partially disordered nanosheets [61,62]. The exfoliation process can be

either physical or chemical one, with the latter often employed in preparing disordered nanosheets. In the process of chemical exfoliation (Fig. 5a), some blocking factors such as quick reaction [63], modified ions [64], functional groups or molecules [65] can weaken the van der Waals forces. This in turn leads to changes in the bond length, bond angle and the ion position within the cell, resulting in the formation of the disordered substance. By means of the chemical exfoliation method, a high-quality ultrathin disordered 2D nanosheet was prepared to serve as a separator in lithium-sulfur batteries. The separator exhibited improved electrochemical properties, mechanical properties, and thermal conductivity [66].

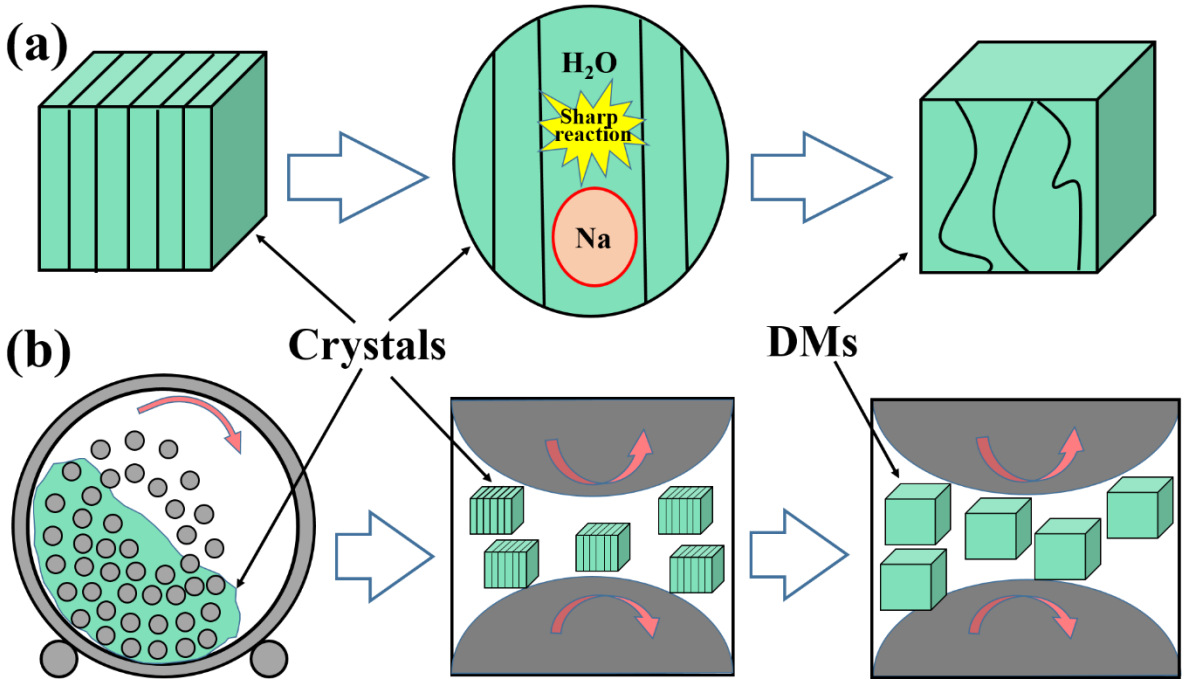

Fig. 5. Schematic illustration of the formation process of DMs by (a) exfoliation method and (b) ball milling method.

2.2.4 Ball milling method

Ball milling is a widely used method to produce DMs by grinding the crystal materials into powders [67,68]. During this process, the powders are subjected to constant impact and friction caused by the grinding balls, resulting in a gradual breakdown of the crystal structure. Furthermore, the milling will introduce some structural defects. Breaking down the crystal structure and introducing defects both increase the free energy of the materials, causing a transformation from crystals to disordered substances (see Fig. 5b) [69]. Using this method, Xiong et al. successfully prepared the disordered/ordered $NaFePO_4$ composite used as a cathode for sodium-ion batteries. The degree of its disorder was elevated by extending the milling time [10].

3. Characterizations and Applications of DMs in LIBs

DMs, serving as anodes, cathodes, solid-state electrolytes and protective layers, play a crucial role in the development of LIBs with high energy density and long cycling stability. The recent progress in the applications of DMs in LIBs will be discussed in detail in this section, with a focus on both the active materials for electrodes and the solid-state electrolytes. The discussion contributes to a comprehensive understanding of the impact of DMs on the energy density, power density, cycle life, and safety of LIBs.

3.1. DMs-based cathodes

3.1.1 Organic disordered cathode materials

Organic materials, found abundantly in nature, are renewable resources of great variety [70,71]. Constructed from light elements like carbon, hydrogen, and oxygen, organic materials exhibit a promising theoretical specific capacity as cathode materials for LIBs and are therefore being widely studied [72]. Due to their high glass-forming ability and production conditions, a significant proposition of organic materials exists in a disordered state. Conjugated microporous polymer (CMP) is a representative type that holds large potential for use as a cathode for LIBs [73,74]. Yang et al. prepared disordered fluorinated covalent quinazoline network-type CMP materials through ionic thermal condensation [75]. Their high nitrogen content (23.49 wt%), extended π-conjugated architecture, layered structure and bipolar combination of benzene and tricycloquinazoline all contributed to CMP's capability to deliver high capacity (250 mAh g^{-1} at 0.1 A g^{-1}) and superior rate cycling properties (115 mAh g^{-1} after 2000 cycles at 2 A g^{-1}). Molina et al. prepared a CMP material based on anthraquinone moieties via a combined miniemulsion-solvothermal method [76]. This resulting CMP material exhibited resilient conjugated microporous and mesoporous nanostructures with remarkably high specific surface area (2200 m^2 g^{-1}). Benefiting from these structural features, the initial discharge capacity of this CMP cathode was 82 mAh g^{-1} at 2C and remained 46.7 mAh g^{-1} after 9000 cycles.

In contrast to crystalline organic materials, their disordered counterparts offer comparative advantages as cathode materials for LIBs. Zheng et al. synthesized covalent crystalline and disordered polymers cathode material-based on tetramino-benzoquinone, i.e., CCP and CAP, respectively [77]. CAP showed higher reversible capacity (~140 mAh g^{-1}) and Coulombic efficiency (approximately 100%) than those of CCP at a low temperature of –60 ℃ (Fig. 6a). The impressive enhanced electrochemical performances of CAP were possibly attributed to its

relatively low impedance value (Fig. 6b) of CAP, ensuring fast Li^+ transport kinetics. The structural origin of this enhancement could be related to the channel-rich disordered structure revealed by the molecular dynamics (MD) simulation (Fig. 6c).

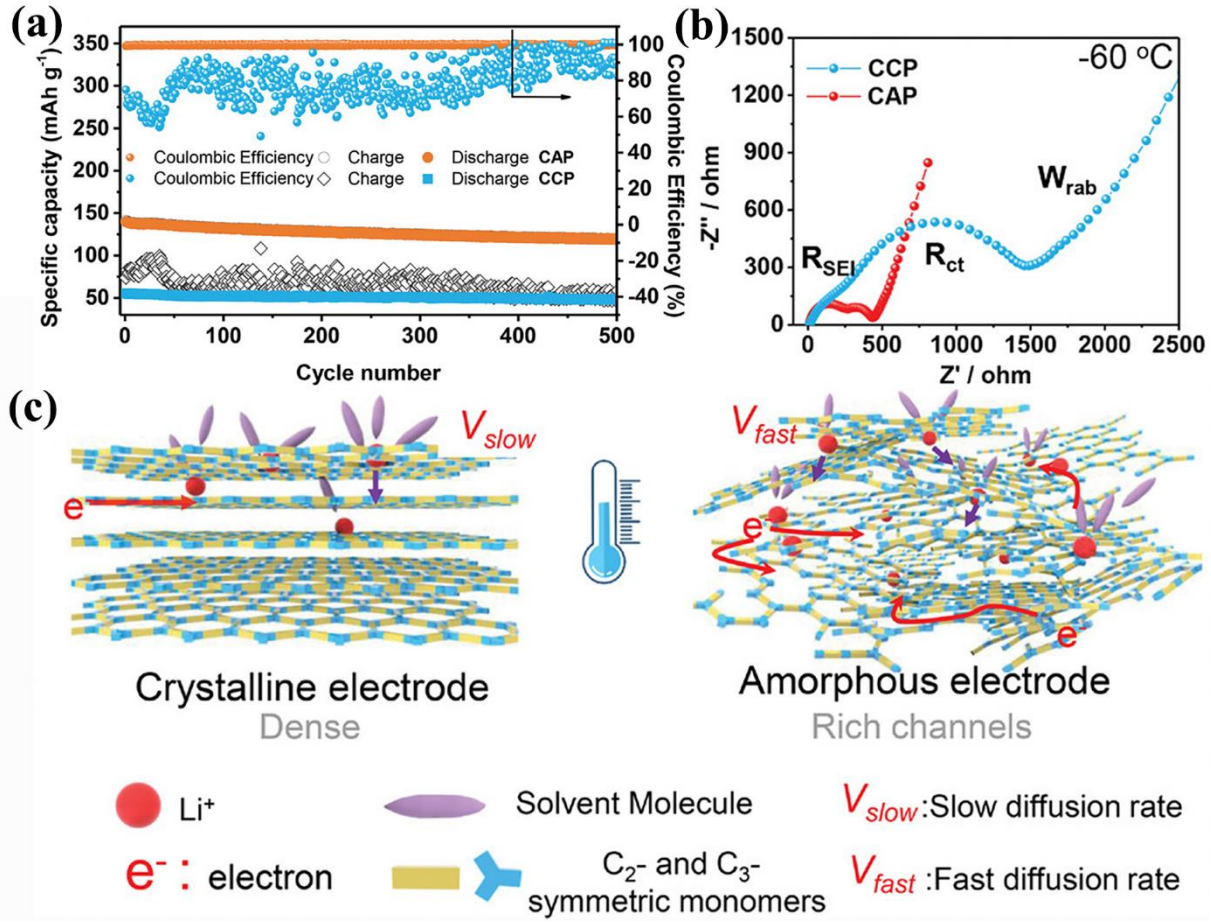

Fig. 6. (a) Comparison of cycle performance of CAP or CCP-based LIBs at the low temperature of –60 °C. (b) Typical Nyquist plots of CAP (red) and CCP (blue). (c) Schematic diagram of the reasons for the difference in low-temperature performance between crystalline and disordered electrodes. Reprinted with permission from Ref. [77]. Copyright 2021, Wiley-VCH.

3.1.2 Disordered vanadium oxide cathode materials

V_2O_5 is considered to be a promising cathode material for LIBs owing to its high theoretical specific capacity (437 mAh g^{-1}) and low cost [78,79]. However, the irreversible phase change (from γ- to ω-phase) of crystalline V_2O_5 could cause a significant capacity loss at the first discharge. Even at a relatively low current density of 10 mA g^{-1} for 10 cycles, the capacity diminishes to half of its initial capacity. This significantly hampers the practical application of V_2O_5 cathode [80]. In contrast, Christensen et al. found that the disordered ω-phase V_2O_5 could deliver a reversible capacity of 310 mAh g^{-1} without reverting to the crystalline state upon charging [81]. This finding implies that the disordering strategy is an effective way to solve the problem of rapid capacity decay of the crystalline V_2O_5 cathode. Xie et al. deposited disordered

V_2O_5 on a multi-walled carbon nanotube paper by the atomic layer deposition (ALD) technique [82]. The disordered composite cathode material exhibited a capacity of 400 mAh g^{-1} after 15 cycles at a current density of 100 mA g^{-1} in LIBs. Mattelaer et al. deposited amorphous/crystalline (a/c)-V_2O_5 and -VO_2 on silicon micropillar arrays using the ALD technique along with precise heat treatment (Fig. 7a) [83]. The reversible capacity of the a-VO_2 cathode was higher than that of the c-VO_2 cathode and was much higher than that of c-V_2O_5 at any current rate due to the absence of irreversible phase change during charging/discharging cycles (see Figs. 7bc). This confirms the superiority of the disordered state of vanadium oxides over the crystalline one in improving the electrochemical performances, especially the cycling stability.

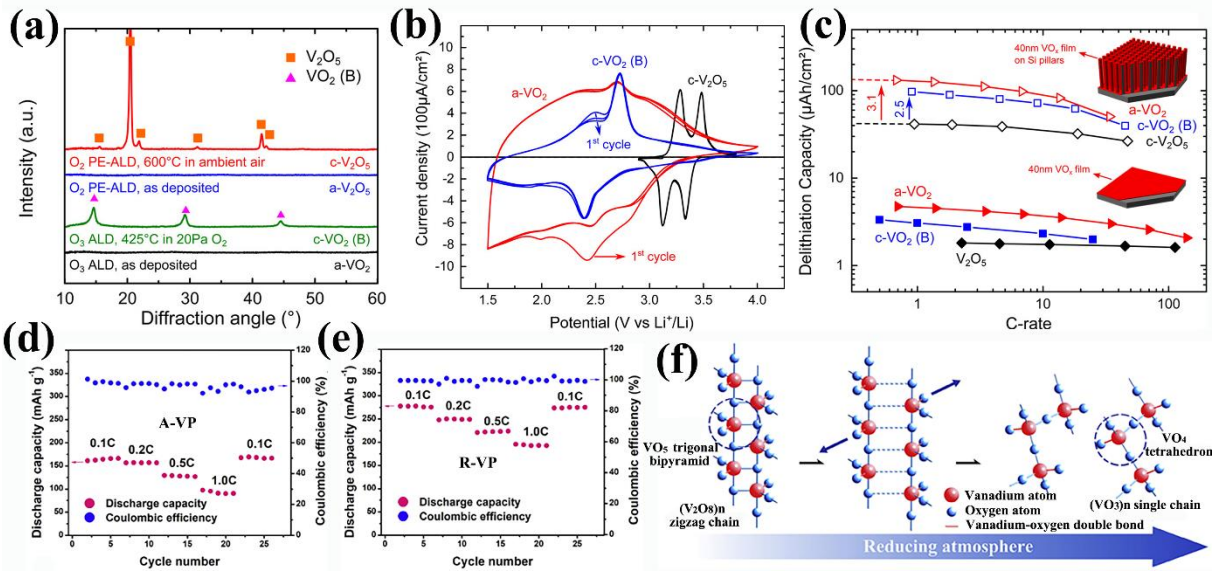

Fig. 7. (a) XRD patterns recorded before and after crystallization of the films. (b) Cyclic voltammograms and (c) rate capability for planar and micropillar electrodes of 40 nm c-V_2O_5 (black), a-VO_2 (red), and c-VO_2 (B, blue) films, coated on silicon micropillar substrates. The potential was varied at 1 mV s^{-1}. Reprinted with permission from Ref. [83]. Copyright 2017, Elsevier. Rate performance of (d) A-VP and (e) R-VP at different current rates. (f) The transition between VO_5 trigonal bipyramid $(V_2O_8)_n$ zigzag-chains and VO_4 tetrahedrons $(VO_3)_n$ single-chains structures. Reprinted with permission from Ref. [84]. Copyright 2019, Elsevier.

In addition to the disordered V_2O_5 materials described above, some V_2O_5-based glasses are also electrochemically active electrode materials. Recently, Li et al. developed a series of glassy V_2O_5-based cathodes for LIBs. They found that the high-rate and cycling performances of the V_2O_5-P_2O_5 glass cathode prepared under a reducing atmosphere (marked as R-VP) were significantly better than that of the one prepared under an air atmosphere (marked as A-VP) (Figs. 7de) [84]. Compared to the A-VP glass, the zigzag chain structure of the R-VP was easily transformed into VO_4 and V_2O_7 units during melting (Fig. 7f), and the network consisting of

these units provided more channels for Li^+ transport. In addition, the reducing atmosphere is in favor of the formation of a lower valence state of V, thus leading to the enhancement in electric conductivity. The same phenomenon was also observed in other vanadium-based glass cathode materials, e.g., V_2O_5-Li_3PO_4-Ca and V_2O_5-Li_3PO_4-BMo_2 glasses [85,86].

Interestingly, the charging/discharging cycling can induce the formation of nanocrystals in the V_2O_5-$LiPO_4$ glass cathode, thereby enhancing the electrochemical performances such as initial specific capacity and high-rate performances [87,88]. Note that the disorder-order engineering was first proposed by some of the present authors to enhance the performances of V_2O_5-TeO_2 glassy anode materials [11,12], as described in chapter *3.2.2*.

3.1.3 Poly-anion disordered cathode materials

Poly-anionic materials as a typical class of cathodes for LIBs have drawn significant attention owing to their superior thermal stability and ionic conductivity, suitable operating voltage, and excellent safety [89,90]. However, the poly-anionic crystal cathodes suffer from a serious issue of high-volume expansion during lithiation [91]. To address this issue, disordering engineering is an effective method to develop poly-anion cathode materials for LIBs.

As a representative of polyanion-type materials, disordered $FePO_4$ (AFP) has attracted considerable attention of battery scientists owing to its high theoretical capacity (~178 mAh g^{-1}), low cost, environmental friendliness, and intrinsic thermal safety [92,93]. Generally, AFP can be obtained by thermal treatment of commercially available disordered $FePO_4 \cdot 2H_2O$. The open disordered network structure of AFP enhances the electronic conductivity and lithium-ion diffusion, leading to improved rate capability of AFP cathode [94]. Nonetheless, the AFP cathode suffers from low electronic and ionic conductivity. To overcome this problem, the incorporation of conductive agents into AFP has been recognized as a promising approach to improve electronic conductivity, and hence the electrochemical performance of the AFP cathode. Lu et al. designed a hierarchical 3D AFP/carbon nanotube (CNT) composite through a micromixer to achieve homogeneous co-precipitation [95]. As shown in Figs. 8ab, this cathode material showed neither a pronounced charge-discharge platform nor redox peaks, characterizing the disordered nature. The 3D heterogeneous conductive network (Fig. 8d) composed of CNT and carbon black (CB) enabled the AFP/CNT composite cathode to exhibit high reversible discharge capacities (175.6 mAh g^{-1} at 0.1C and 139 mAh g^{-1} at 5C) and superior cycling stability (no apparent capacity degradation after 500 cycles at 5C) (Fig. 8c). Zhang et al. prepared a uniformly dispersed AFP/CNT nanocomposite using a mild sonication-

assisted micromixer synthesis method [96]. The resulting cathode material exhibited capacities of 162 and 117 mAh g^{-1} at 1C and 5C, respectively. In addition, Mo et al. prepared a 3D holey-graphene (HG) framework cross-linked with encapsulated mesoporous AFP nanoparticles (denoted as MFPO/HG) for LIBs by applying a hydrothermal assisted self-assembly strategy (Figs. 8ef) [97]. The presence of a large number of pores embedded in graphene nanosheets (Fig. 8g) can significantly increase the contact area between the electrode and the electrolyte, thereby enhancing the efficiency of Li^+ transport. Through the synergistic effect of both the unique structure and the good conductivity of graphene, the MFPO/HG exhibited a high-rate capability (76 mAh g^{-1} at 50C) and remarkable cycle stability (92.5% reversible capacity retention over 1000 cycles) (Fig. 8h).

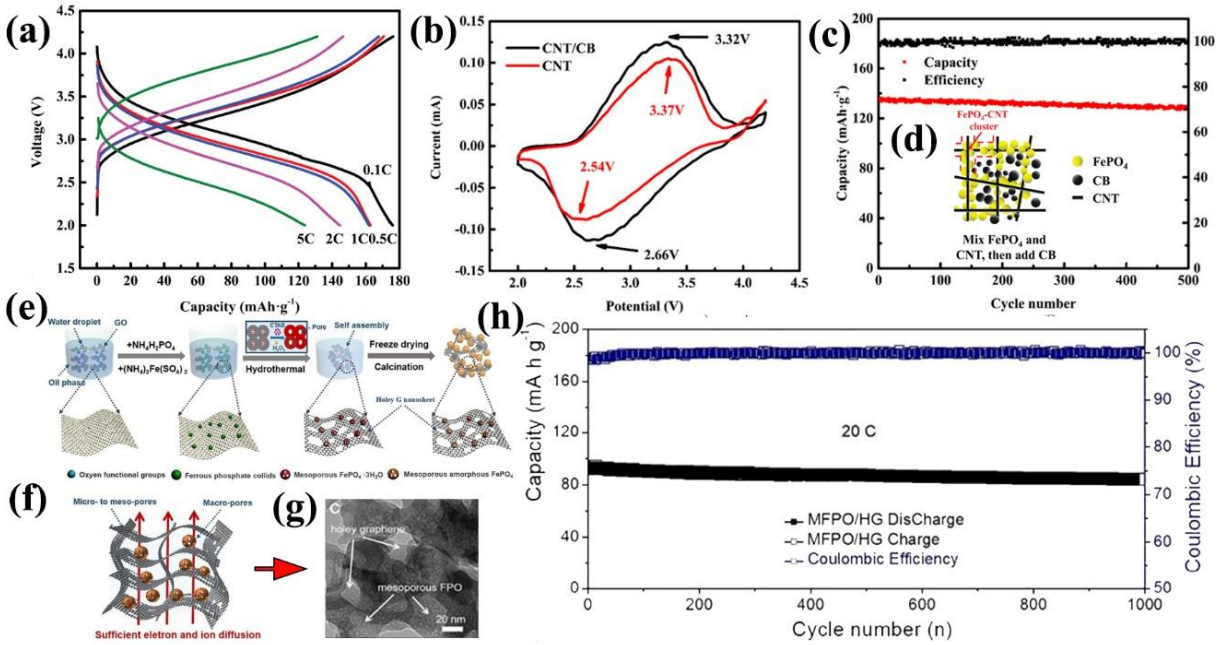

Fig. 8. (a) Charge-discharge profiles of $FePO_4$/CNT composite at current rates ranging from 0.1 to 5C. (b) Cyclic voltammetry (CV) curves of $FePO_4$ cathodes with CNT/CB and single CNT additives. (c) Cycling performances and Coulombic efficiency of $FePO_4$/CB-CNT cathodes at 5C. (d) Schematic diagram of $FePO_4$/CB-CNT microstructure. (a-d) Reprinted with permission from Ref. [95]. Copyright 2019, ACS. Schematics illustrating the synthesis of MFPO/HG (e) and the ion/electron conductive pathways and spatial arrangement of the electrode materials in MFPO/HG cathode (f). (g) TEM image of MFPO/HG architecture. (h) Cycling stability of MFPO/HR electrode under 20C for 1000 cycles. (e-h) Reprinted with permission from Ref. [97]. Copyright 2021, Elsevier.

Table 1. Summary of electrochemical performance of disordered cathode materials for LIBs.

Prototype construction	Specific disordered materials	Highest specific capacity/rate (mAh g^{-1}/mA g^{-1})	Voltage window (V)	Rate performance (mAh g^{-1}/mA g^{-1})	Cycling performance [mh g^{-1}/cycle numbers (N)/mA g^{-1}]	Ref
Organic based	dibromotetraoxapentacene	108/120	3.0-4.8	71.4/6000	-	[73]
	fluorinated covalent quinazoline networks	250/100	1.5-4.5	105/5000	115/2000/2000	[75]
	anthraquinone moieties	104/149	1.5-3.5	82/198	21.3/80000/4470	[76]
	tetramino-benzoquinone-cyclohexanehexaone dimer	162.8/50 at –60 ℃	1.5-3.5	100/1000	~120/500/100	[77]
Vanadium oxide based	V_2O_5/CNT paper	400/100	1.5-4.0	~300/2000	300/100/100	[82]
	V_2O_5-P_2O_5 glass	342/17	2.0-4.2	193/170	175/300/85	[84]
	65V_2O_5-30Li_3PO_4-5BMo_2 glass	289.9/50	1.5-4.2	102/500	246.9/50/50	[85]
	75V_2O_5-25Li_3PO_4-20%CaC_2 glass	319.3/100	1.0-4.0	-	280.3/100/100	[86]
	Li_3PO_4-V_2O_5-LiF glass	344.3/50	1.5-4.2	120/800	269.7/200/50	[87]
	70V_2O_5-30P_2O_5 glass	269.4/50	1.5-4.2	118.1/100	227.4/50/50	[88]
Poly-anion based	$FePO_4$ nanosheets	185/17.8	2.0-4.2	107/356	181/400/17.8	[93]
	$FePO_4$	147/85 at 80	2.0-4.3	-	~120/20/85	[94]
	$FePO_4$	153/0.1 mA cm^{-2}	2.0-3.9	-	-	[98]
	$FePO_4$/CB-CNT	175.6/17.8	2.0-4.2	139/890	~130/500/890	[95]
	$FePO_4$/CNT	162/17.8	2.0-4.2	117/890	~105/2000/890	[96]
	$FePO_4$/graphene	156/89	2.0-4.0	76/8900	~72/500/8900	[97]
	Li_4NiPO_6	330/320	2.0-4.8	240/9600	-	[99]
	1.3LiF-$FeSO_4$	~130/0.2 mA cm^{-2}	2.5-4.3	125/1.0 mA cm^{-2}	130/30/0.2 mA cm^{-2}	[100]
	$Li_2Fe_{0.94}Ti_{0.06}SiO_4$/C/MWCNT	240/238	1.5-4.8	138/3320	157/1000/332	[101]
	$Na_2Fe(PO_4)_3(CO_3)$	128/10	2.0-4.2	40/2000	91/150/50	[102]

In addition to the AFP cathode, there is intensive research on the disordered $LiMPO_4$ (where M can be Mn, Fe, Co, Ni, etc.) within the category of poly-anion cathodes. Indeed, these materials hold promise due to their advantageous features, including high theoretical specific capacity, cost-effectiveness, eco-friendliness, and inherent thermal stability. Sabi et al. prepared a series of disordered $Li_xM_yPO_z$ cathode materials by a sputtering method and measured their electrochemical properties as a function of composition [99]. It was found that the disordered LiNiPO cathode exhibited the highest capacity of 330 mAh g^{-1} at 1C. Since the redox potential of poly-anionic cathodes depends on the type of the anion groups, the cathode performance can be improved by adjusting the proportion of the tetrahedral anion groups or their derivatives in poly-anionic-like disordered materials, such as SO_4^{2-} [100], SiO_4^{2-} [101], CO_3^{2-} [102]. Table 1 displays the electrochemical performances of the above-mentioned AM cathodes for LIBs.

3.2 DM-based anodes

According to their reaction mechanisms, anodes can be classified into three main categories: intercalation-, conversion-, and alloying-type anode [103,104]. In general, crystalline anodes inevitably undergo significant volume expansion during electrochemical processes, presenting a major challenge in the development of novel anode materials. From a microstructural perspective, DMs are a promising alternative to their crystalline counterparts. This is because the DMs can sustain part of the volume expansion induced by their reaction with Li during the charging and discharging process [105]. This section discusses the recent progress made in the disordered anode materials.

3.2.1 Intercalation-type anode materials

Carbon and titanium-based materials, including TiO_2 and $Li_4Ti_5O_{12}$, are two crucial candidates for fabricating the intercalation-type anodes [106,107]. These anode materials allow for reversible intercalation/extraction of lithium ions from their interlayer space [108]. In contrast to crystalline materials, DMs possess abundant interlayer space, multiple defects, and strong stability. These characteristics are highly beneficial to the storage and transfer of lithium ions.

Currently, carbon is the most commonly used anode material due to its advantageous features, including high specific surface area, tunable porous structure, diverse morphologies, and high electronic conductivity [109]. In the scope of disordered carbon-based materials, an important subject is to improve the electrochemical performance through the smart design of morphology and pore structures by adjusting synthesis parameters [110]. Liang et al. synthesized a disordered CNT anode material through pyrolysis of sulfonated polymer nanotubes/SiO_2 hybrids under varying atmospheric conditions [111]. They found that the disordered CNTs

synthesized in a N_2-H_2 atmosphere exhibited an ideal pore structure with abundant defect sites, resulting in outstanding lithium storage performances with a capacity of 400.6 mAh g^{-1} at 2 A g^{-1} after 200 cycles and 212.1 mAh g^{-1} at 10 A g^{-1} after 400 cycles. Apart from the synthesis atmosphere, the carbonization temperature stands as a crucial factor that influences the morphology of disordered carbon (Fig. 9a) [112]. Wang et al. found that the disordered carbon nanosheets obtained at the carbonization temperature of 800 °C displayed a capacity of 579 mAh g^{-1} at 2 A g^{-1} after 900 cycles. (Fig. 9b). This outstanding cyclability surpasses that of a large number of previously reported carbonaceous electrodes and could compete with that of the heteroatom-doped carbon anodes [113,114]. Yang et al. synthesized a 3D porous disordered carbon using the pyrolyzing sucrose method. This anode delivered a high reversible specific capacity of 400 mAh g^{-1} at a current density of 50 mA g^{-1} owing to the increased adsorption site for Li^+ ions within the investigated potential range (0.01-3.0 V) [115]. Furthermore, the synergy between the disordered carbon and other high-specific capacity nanocrystal materials is also a focusing point in the development of anode materials [116,117]. In addition, as a typical disordered carbon material, hard carbon has also gained continuously growing attention in the field of energy storage [118] due to its large interlayer spacing (>0.34 nm) and a low working potential [119]. In particular, as anode materials for Na^+ ion batteries, hard carbon materials can provide more active sites for sodium storage by means of nanostructure design [120] and heterogeneous element doping [121].

Additionally, a disordered Ti-based material, which belongs to the intercalation-type anode category, has undergone extensive research [122,123]. Liu et al. prepared disordered mesoporous TiO_2 nanosheets as anode materials using potassium chloride as a template [124]. Its unique structure could effectively accommodate stress without pulverization after 1000 cycles and maintained a reversible capacity of 103 mAh g^{-1} at 6 A g^{-1}. However, nanosheets are prone to agglomeration due to their high surface energy. To address this issue, Qi et al. prepared disordered TiO_2 porous nanosheet aerogels by a surfactant-free assembly technique [125]. Thanks to the porous aerogel structure, the disordered TiO_2 anode exhibited a capacity of 310 mAh g^{-1} at 1 A g^{-1} after 300 cycles, which was considerably higher than that of crystalline TiO_2. Yuwono et al. compared the storage mechanism of Li^+ between disordered and ordered TiO_2 anode materials [126]. The diffusion energy barrier of Li^+ in disordered TiO_2 was found to decrease with the increasing molar fraction of lithium. Moreover, the loose structure of disordered TiO_2 provided more lithium storage sites than its ordered counterpart.

Integrating materials with high theoretical capacity into the TiO_2 matrix is an effective approach to further enhance the capacity of the disordered TiO_2-based anode materials. For

example, Lai et al. proposed a novel 3D porous core-shell carbon fiber (PCSF) scaffold containing well-dispersed disordered TiO_2 and disordered SiO_2 with high specific capacity (~1965 mAh g^{-1}) [127]. The Li@PCSF anode material with heterostructure was obtained by further Li plating. The morphology of the Li layer deposited on the carbon fibers was determined by the plating capacities (i.e., the amount of deposited Li) (Figs. 9c-f). Through the density functional theory calculation, the authors found that lithium preferentially entered the pores of the fibers until saturation, followed by deposition on the outer surface of the fibers (as presented in Fig. 9g). The Li@PCSF, Li@Cu, and Li@carbon fiber (CF) anodes were, respectively, assembled to full cells being paired with $LiNi_{0.5}Co_{0.2}Mn_{0.3}O_2$ (NCM) cathodes. The Li@PCSF/NCM full cell exhibited the best rate performance (Fig. 9h).

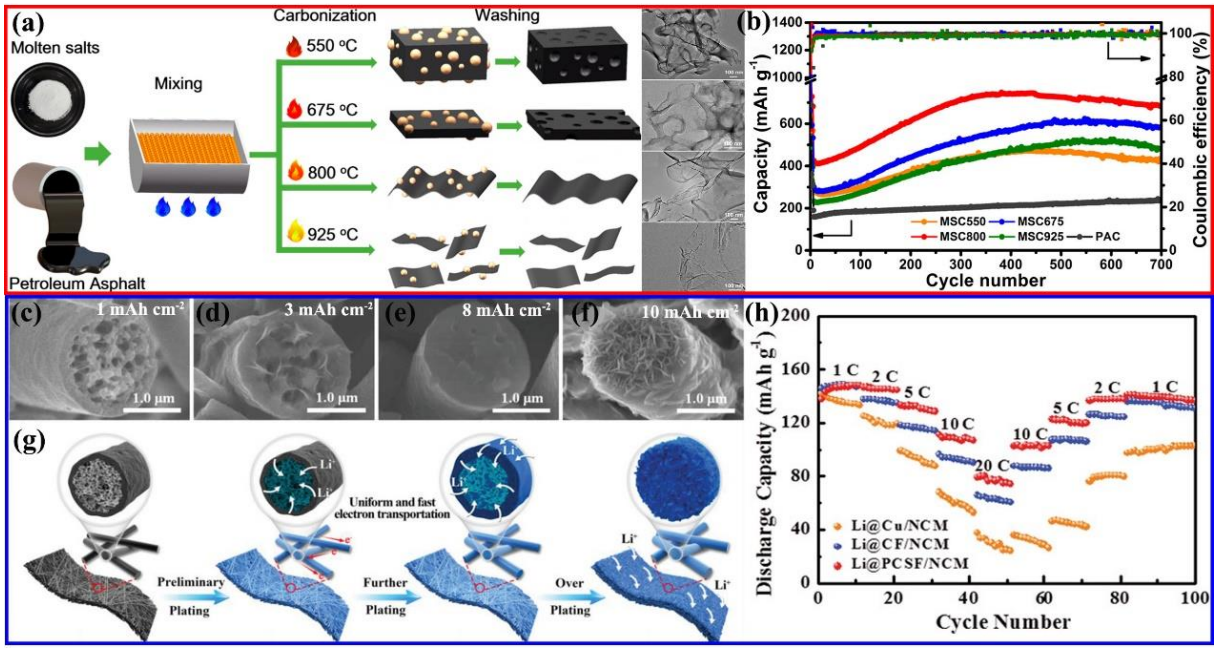

Fig. 9. (a) Schematic illustration of the evolution process of molten-salt carbons (MSCs). (b) Cycling performance at a current density of 1 A g^{-1} of MSCs with different preparation conditions and PAC. (a, b) Reprinted with permission from Ref. [112]. Copyright 2018, ACS. Cross-sectional SEM images of the PCSF host after plating (c) 1 mAh cm^{-2}, (d) 3 mAh cm^{-2}, (e) 8 mAh cm^{-2} and (f) 10 mAh cm^{-2}. (g) Schematic illustration of the Li plating in the PCSF host at different states. (h) Cycling performance of Li@PCSF/NCM full cells. (c-h) Reprinted with permission from Ref. [127]. Copyright 2019, ACS.

3.2.2 Conversion-type anode materials

It is known that the conversion-type (CT) anode materials exhibit higher theoretical specific capacities than the insertion-type anode materials. The CT anode is mainly composed of elements from Group IVA and VA of the periodic table, along with their corresponding compounds including oxides, sulfides, nitrides, phosphides, and selenides. In this section, we review the recent advances in the development of CT-disordered materials for LIBs.

Fe_2O_3 has been regarded as an attractive anode for LIBs, owing to its low cost, high electrochemical activity, and high theoretical capacity (1007 mAh g^{-1}) [128]. Zhao et al. fabricated button-shaped disordered Fe_2O_3/rGO/carbon nanofiber film as a freestanding flexible anode for LIBs [129]. Benefitting from its outstanding reversibility of the conversion reaction of disordered Fe_2O_3, unique hierarchical structure, and high electronic conductivity, the Fe_2O_3/rGO/carbon nanofiber film anode presented a high reversible capacity of 811 mAh g^{-1} at 0.1 A g^{-1} and a remarkable rate performance, i.e., a capacity of 584 mAh g^{-1} after 400 cycles at 2 A g^{-1}.

Another example of CT-disordered anode materials (CT-DAMs) is molybdenum trioxide (MoO_3), which is a promising anode candidate for LIBs thanks to its high electronic conductivity [130]. Yan et al. synthesized a disordered-MoO_{3-x}@Ti_3C_2-MXene material with a 2D non-van-der-Waals heterogeneous structure for LIBs [131]. As shown in Fig. 10a, the disordered MoO_3 was uniformly anchored on Ti_3C_2-MXene. Due to the weak interactions between the adjacent disordered MoO_{3-x} layers, the lithium storage was caused by two diffusion modes of Li^+ ions, i.e., 1) the capacitor-like diffusion on the surface of the disordered layer and 2) the diffusion-controlled mode within the disordered layer. The former one was confirmed to give a larger contribution to high-rate performance (Fig. 10b). Wu et al. compared the electrochemical properties between the ordered and disordered MoO_3 anodes for LIBs [132]. The disordered MoO_3 showed better performances than the crystalline counterpart due to its rapid ion transport and more active sites.

Yue et al. have proposed a disorder-order engineering concept to enhance their electrochemical performances of the V_2O_5-TeO_2 based glass anodes in LIBs [10-14,16]. They selected this glass system because it demonstrates high electronic conductivity, tunable composition, and the capacity to intercalate lithium ions [11,133,134]. The nanocrystals and the remaining glass matrix gave a synergetic effect to facilitate the ionic and electronic transport and to maintain the glass structure stable against discharging/charging. As a result, both the capacity and cycling stability were greatly enhanced, maintaining 124 mAh g^{-1} after 5000 cycles at a current density of 1 A g^{-1}. The structural origins of both the electrochemical reaction-induced nanocrystallization and structural stability were clarified by means of the state-of-the-art solid-state nuclear magnetic resonance (SSNMR) [15]. Upon the lithium interaction and extraction, the glass network was first dissociated into isolated units and then transformed into different types of ordered nanostructured clusters (Fig. 10e). In addition to examining the electrochemical properties, a comprehensive characterization of the mechanical and dynamic properties of V_2O_5-TeO_2-P_2O_5 glasses was conducted, contributing to optimizing the various

performances of glass anodes [135]. The disordered-order engineering concept has been successfully applied to other oxide glass anodes [136-143], MOF-based glass anodes [13,14,16] and polyanion-based cathodes [10,144]. It should be noted that the MOF glass utilized for constructing the anodes in [16] was a cobalt-based zeolitic imidazolate framework (ZIF) glass, namely ZIF-62 glass [145]. The disorder-order engineering strategy, combining the unique advantages of both ordered and disordered structures, holds great promise as a crucial pathway for advancing electrode materials specifically for LIBs.

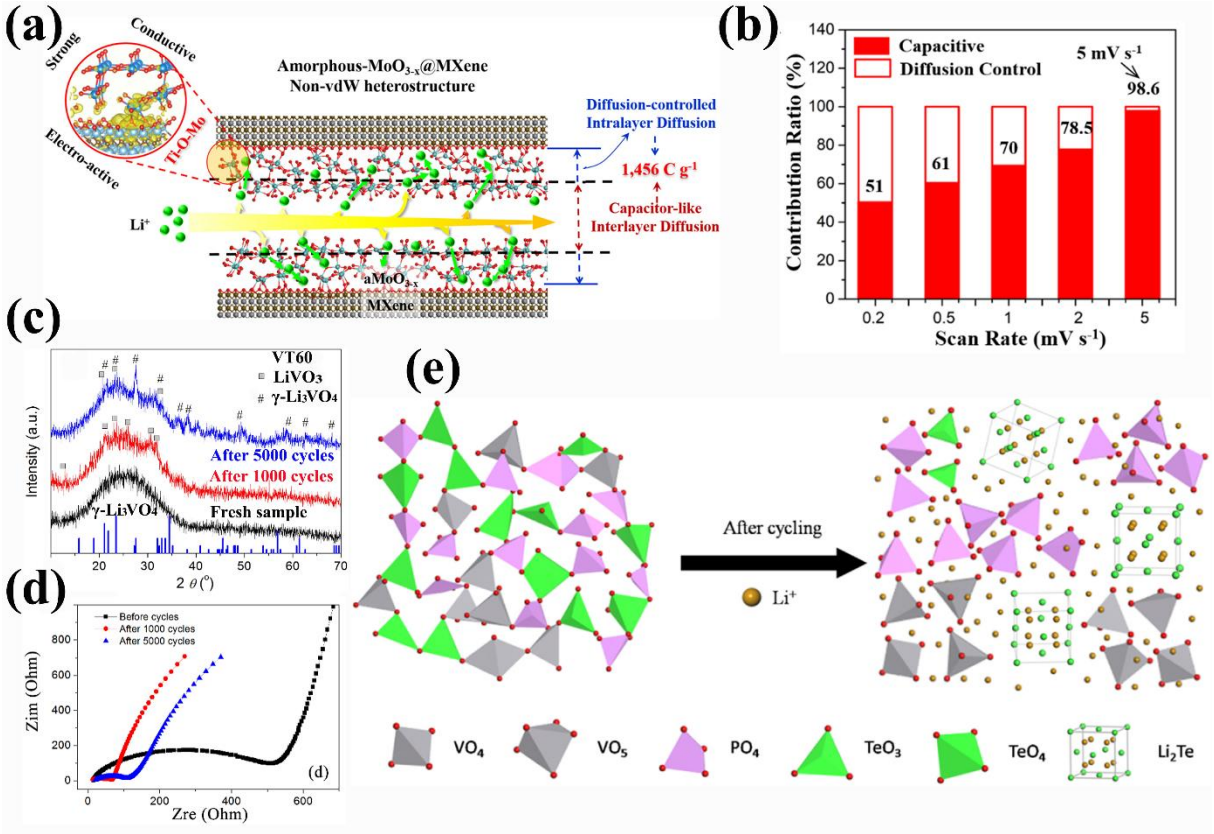

Fig. 10. (a) Illustration of facile capacitor-like interlayer diffusion and diffusion-controlled intralayer diffusion. (b) Capacitive contribution ratios at different scan rates. (a, b) Reprinted with permission from Ref. [131]. Copyright 2021, Elsevier. The XRD analysis (c) and Nyquist plots (d) of the fresh (ball milled) VT60 glass, the VT60 glass anode after 1000 and 5000 discharging/charging cycles at a current density of 1 A g^{-1} and the γ-phase Li_3VO_4 crystal. (c, d) Reprinted with permission from Ref. [12]. Copyright 2019, Elsevier. (e) Schematic representation for the local structural evolution induced by cycling. Reprinted with permission from Ref. [15]. Copyright 2021, Elsevier.

Disordered FeP is another attractive conversion-type anode material. Zheng et al. designed a 3D flake-carbon nanosheets (CNs)-like configuration through confining disordered FeP nanoparticles into ultrathin 3D interconnected P-doped porous carbon nanosheets (denoted as FeP@CNs) [146]. The FeP@CNs anode exhibited the reversible capacity of 956 mAh g^{-1} at 1 A g^{-1} without obvious capacity decay for 500 cycles (Fig. 11a). Additionally, it showed superior cycling stability, maintaining capacity retention of 98% even after 2500 cycles at 4 A g^{-1}) (Fig.

11b). These performance levels surpassed those of both pure CNs and pure FeP anodes. The 3D-interconnected CNs in FeP@CNs facilitated rapid electron/ion-transport kinetics. The disordered FeP with intrinsic buffering voids offered abundant lithium storage sites and preserved space to accommodate the expansion of active materials during cycling (Fig. 11c). In addition to disordered FeP, other conversion-types of disordered anode materials, such as ZnP_2 [147], Fe_2N [148] and FeSe [149], are currently under intensive investigation.

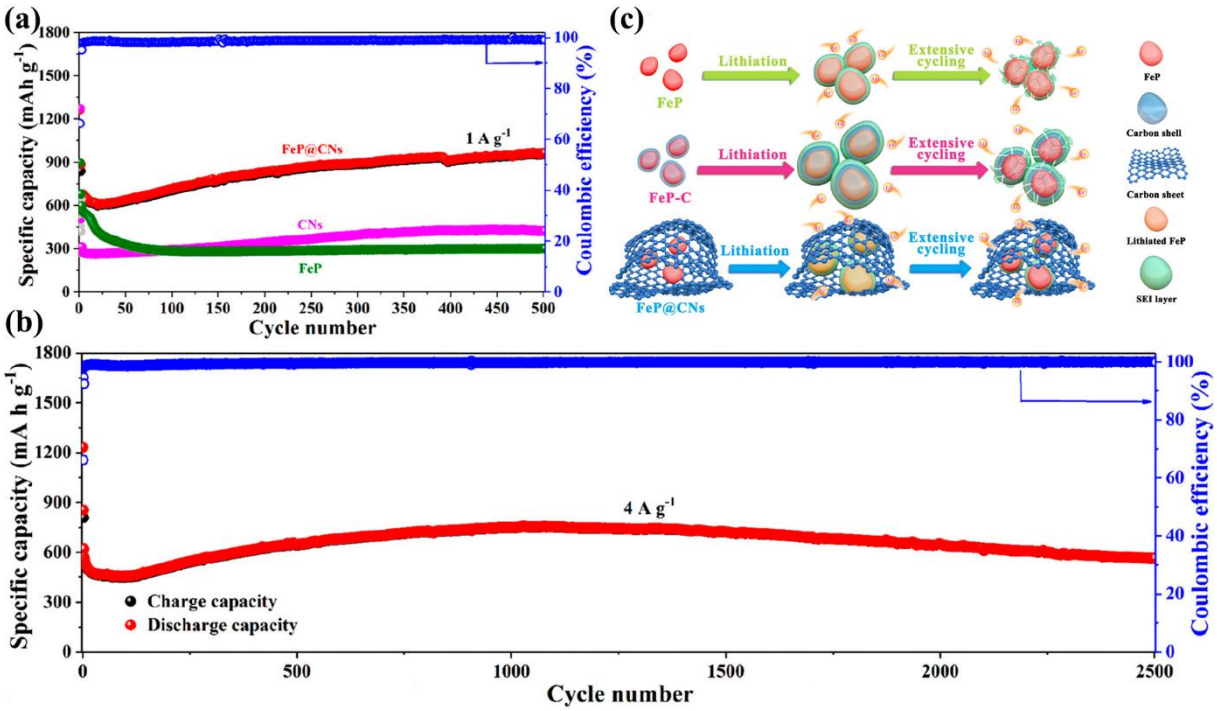

Fig. 11. (a) Cycling performances of FeP@CNs, CNs and bare FeP electrodes at 1 A g^{-1}. (b) Schematic illustration of the morphology evolutions of bare FeP nanoparticles, FeP-C and FeP@CN electrodes. (c) Long-term cycling performance of FeP@CNs electrode at 4 A g^{-1}. (c-e) Reprinted with permission from Ref. [146]. Copyright 2020, ACS.

3.2.3 Alloying-type anode materials

Silicon (Si), germanium, silicon monoxide, and tin oxide are among the materials capable of reacting with lithium through an alloying/de-alloying mechanism [150]. Although these alloying-type materials exhibited a higher specific capacity than commercial graphite, their short cycling life and large irreversible capacity at the initial cycle limited their applications in LIBs [151]. To address this problem, amorphization of these materials is one of the most promising solutions. Si is well-known with a high theoretical specific capacity of 4200 mAh g^{-1}, but its huge volume change and low electronic conductivity hindered its practical application. In this section, we use Si anode as a typical case to review the recent progress in studying the disordered alloying-type anode materials.

Due to their disordered and loosely connected network structure, disordered Si anodes showed advantages over their crystalline counterparts in mitigating volume changes during

cycling [152]. Due to their disordered and loosely connected network structure, disordered silicon anodes exhibit advantages over their crystalline counterparts in mitigating volume changes during cycling. It is important to note that the disordered Si anode is mainly utilized in the form of thin films. The electrochemical performances of these films depend on their thickness. Generally, in the way that thinner films tend to yield better performances [153]. In this regard, disordered Si is usually compounded with other materials to improve the electrochemical performance. For instance, Cui et al. produced core-shell silicon nanowires with an ordered-disordered structure to be used as an anode for LIBs. Specifically, the ordered Si cores serve as a stable mechanical support and an efficient electrical conducting pathway, whereas the disordered shells store Li^+ ions. This combination results in outstanding cycling performance, achieving approximately 1000 mAh g^{-1} with a retention of about 90% of capacity over 100 cycles [154]. Similarly, Wei et al. fabricated a Si/SiO_x anode material with a disordered/ordered heterostructure that could accommodate the expansion of Si volume and relieve the mechanical stress during the charging/discharging process [155]. This anode delivered a high capacity of 1200 mAh g^{-1} at 8 A g^{-1} and showed nearly 100% capacity retention during long-term cycling at 0.5 A g^{-1}. Zhou et al. conducted a series of investigations in improving SiO_x anode performances through morphology design [156-158]. A monodisperse and homogeneous SiO_x/C microsphere anode exhibited a reversible capacity of 689 mAh g^{-1} at a current density of 500 mA g^{-1} with a capacity retention of 91.0% after 400 cycles [157]. They designed the yolk-shell structured SiO_x/C microsphere anode materials [158], which had large internal voids to accommodate volume changes inherent in SiO_x. Beneficially, this yolk-shell structured SiO_x/C microsphere anode showed excellent rate capability (725 mAh g^{-1} at 1000 mA g^{-1}) and superior cycling stability (972 mAh g^{-1} after 500 cycles at 500 mA g^{-1}). Exploring the evolution of defects within these anodes during cycling could be incredibly intriguing, especially regarding how these changes might influence their electrochemical performance.

While enhancing the electrochemical performance of ordered/disordered heterostructure Si anode, the issue of limited electronic conductivity needs to be urgently addressed. The most commonly used method is to composite Si with other conductive materials [159]. Ryan et al. constructed a core-shell structured $Cu_{15}Si_4$/disordered Si nanowire composite anode (Figs. 12a-c) [160]. The conductive yet electrochemically inactive $Cu_{15}Si_4$ core facilitated the rapid electron transfer between the collector and the disordered Si, resulting in significantly enhanced anode capacities up to 1367 mAh g^{-1} and 1520 mAh g^{-1} at 5C in half cell and full cell, respectively (Figs. 12d-e). The core-shell structured Si anode was also developed by Lin et al. [161]. The graphene nanowalls in the core played a crucial role in improving the electronic

conductivity while the partially disordered Si served as the shell to accommodate volume changes. This anode exhibited a discharge capacity of 1116.2 mAh g^{-1} after 200 cycles at 0.1C, which was significantly higher than that of the pure Si anode (704.2 mAh g^{-1} at 0.1C). The 2D porous disordered silicon nanoflakes were integrated with long multi-walled carbon nanotubes (MWCNTs) to form a flexible freestanding film anode for LIBs (Fig. 12f) [162]. Benefiting from the hierarchical structure of Si (Figs. 12gh), its aggregation and pulverization were greatly alleviated. The carbon nanotubes were capable of establishing highly conductive pathways for lithium ions. This flexible Si-MWCNT anode material exhibited the high capacities of 1664, 1403, 1224, 989, 668, and 381 mAh g^{-1} at current densities of 200, 400, 800, 1600, 3200, and 6400 mA g^{-1}, respectively (Fig. 12i). The electrochemical performances of some disordered anode materials for LIBs are listed in Table 2.

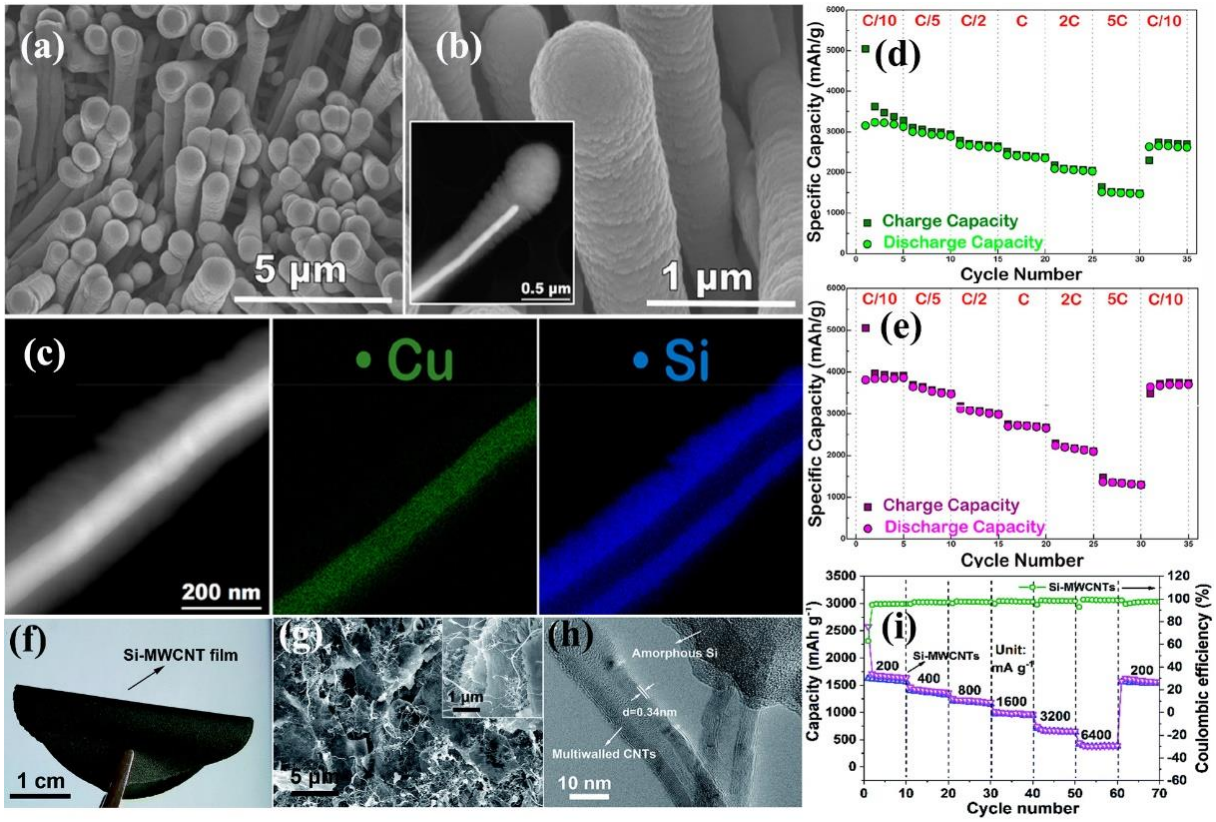

Fig. 12. (a) Low and (b) higher magnification SEM images of the $Cu_{15}Si_4$/Si core/shells NWs. (c) TEM image of the length of a core/shell wire with corresponding EDX elemental maps for Cu (green) and Si (blue). Charge and discharge capacities in half-cell (d) and full-cell (e) were tested at rates of C/10, C/5, C/2, C, 2C, 5C, and C/10. (a-e) Reprinted with permission from Ref. [160]. Copyright 2019, ACS. (f) Digital photo illustration of the freestanding Si-MWCNT film. (g) Cross-sectional SEM images. (h) HRTEM images of the Si-MWCNT film. (i) Rate capability of freestanding Si-MWCNT electrode at various current densities. (f-i) Reprinted with permission from Ref. [162]. Copyright 2020, RSC.

Table 2. The electrochemical performances of disordered anode materials for LIBs.

Reaction type	Specific disordered materials	Highest specific capacity/rate (mAh g^{-1}/mA g^{-1})	Rate performance (mAh g^{-1}/mA g^{-1})	Cycling performance (mAh g^{-1}/N/mA g^{-1})	Ref
Intercalation type	Sulfonated polymer nanotubes/SiO_2	~1130/500	246/8000	212.1/400/10000	[111]
	C nanosheets	~1350/100	283/10000	396/900/5000	[112]
	Porous C	~1470/50	-	~600/120/50	[115]
	Si/Fe_xSi_y@NC/CNTs	1190.1/200	572.0/5000	994.4/600/1000	[116]
	Graphene/IOC@Si	1528.1/100	62/5000	484/450/1000	[117]
	TiO_2 nanosheet	158/200	108/10000	103/1000/6000	[124]
	TiO_2 porous nanosheet	740/100	194.6/2000	310/300/1000	[125]
	SiO_2-TiO_2/porous carbon skeleton	137.8/155	74.2/3100	114.4/200/1550	[127]
Conversion type	Fe_2O_3/rGO/CNFs	~1378/100	664/1000	584/400/2000	[129]
	MoO_{3-x}@Ti_3C_2-MXene	1600/50	139/1000	~500/500/200	[131]
	Ordered/disordered MoO_3 Nanosheets	935/100	100/5000	510/200/1000	[132]
	FeP/Carbon	~1200/200	403/16000	563/2500/4000	[146]
	ZnP_2/C	~1800/100	410/15000	1300/2730/2000	[147]
	Fe_2N@AC@rGO	~880/200	303/10000	505/500/1000	[148]
	FeSeO-C-CNT	~1400/500	560/30000	617/1800/30000	[149]
Alloying type	Ordered-disordered core-shell Si nanowires	~3200/850	807/3400	~800/100/6800	[154]
	Disordered/ordered Si/SiO_x	2500/200	1200/8000	2100/300/500	[155]
	monodisperse and homogeneous SiO_x/C microspheres	999/100	689/500	627/400/500	[157]
	GNW@Si	~2000/190	526.2/9510	-	[161]
	Si/MWCNTs	~2766/200	381/6400	844.9/200/1600	[162]

3.3 Disordered solid-state electrolytes

Organic liquid electrolytes are widely used in LIBs due to their high ionic conductivity and easy accessibility. However, the limited thermal stability of liquid electrolytes poses a significant challenge for most LIBs, potentially leading to battery explosion or flammability [163,164]. Therefore, solid-state electrolytes (SSEs) are perceived as one of the most promising alternatives to conventional organic liquid electrolytes and have attracted great attention [165,166]. However, SSEs need to overcome the challenges of poor interfacial compatibility and low ionic conductivity before they can be used in practice [167,168]. Aiming at these problems, a number of research strategies have been proposed, including the disorder strategy.

Disordered polymers have been extensively explored as electrolyte materials due to their structural flexibility and easy adhesion to the electrodes. Xue et al. synthesized crystalline and disordered poly(ethylene oxide)$_3$:$LiCF_3SO_3$ (PEO_3:$LiCF_3SO_3$) polymer electrolytes, respectively, for LIBs [169]. They found that the transport of Li^+ ions in disordered SSE is faster than that in crystalline SSE since the activation energy of the Li^+ in disordered PEO_3:$LiCF_3SO_3$ (0.6 eV) is lower than that of its crystalline counterpart (1.0 eV). Lin et al. fabricated a 3D cross-linked silyl-terminated disordered polymer electrolyte that exhibited an enhanced ionic conductivity (~0.36 mS cm^{-1}) and thermal stability due to its relatively high melting temperature (T_m=379 °C) [170]. Compared to the disordered organic SSEs, the inorganic electrolytes have better mechanical and thermal properties. Therefore, taking advantage of organic and inorganic SSEs, Self et al. developed a hybrid electrolyte containing high ionic conductive Li_3PS_4 in the disordered state and poly(ethylene oxide) (PEO) binder [171]. A suitable PEO content limited to 1-5 wt.% in these hybrid electrolytes ensured a reasonable Li^+ conductivity (e.g., 1.1×10^{-4} S cm^{-1} at 80 °C) and a satisfactory bond quality.

Apart from the ionic conductivity, the interface compatibility between the SSEs and electrode materials is critically important for ensuring the high electrochemical performance of LIBs [172]. Tian et al. reported a novel interface modification method, which involves embedding $Li_{6.75}La_3Zr_{1.75}Ta_{0.25}O_{12}$ (LLZTO) particles in disordered Li_3OCl [173]. As illustrated in Fig. 13a, a large number of voids formed between pure LLZTO particles, leading to the increased interfacial impedance between the LLZTO and the anode, and hence, facilitating the lithium dendrite growth. The introduction of disorder Li_3OCl into the interfaces between LLZTO particles led to the formation of the ionic-conductive continuous structural network, thereby lowering the interfacial impedance (Fig. 13b). This design provided the disordered composite LLZTO/Li_3OCl SSE with high ionic conductivity (2.27×10^{-4} S cm^{-1}), low interfacial resistance (90 Ω), and excellent thermal stability (T_m=350 °C). Recently, Lai et al. proposed a novel

strategy, by which the Li_2S could in-situ grow on the interfacial layer between the lithium anode and the disordered-sulfide-LiTFSI-poly-(vinylidene difluoride) (PVDF) composite solid electrolyte (SLCSE) [174]. The Li_2S-modified interfacial layer improved the wettability of lithium metal and electrolyte, resulting in the composite electrolyte exhibiting an ionic migration energy barrier as low as 0.22 eV (Fig. 13c), thereby enhancing electrochemical performances of LIBs (Fig. 13d). Zhao et al. engineered the lithium metal-glassy SSE ($Li_2S+SiS_2+P_2O_5$) interface by forming an in-situ interlayer via heat treatment [175]. The good compatibility between the electrolyte and lithium metal ensured that the equipped battery presented a capacity of 2 mA h cm^{-2} at 1 mA cm^{-2} and cycled stably for 1200 h. Likewise, it is important to improve the interface state between the cathode and solid electrolyte in the cell [176].

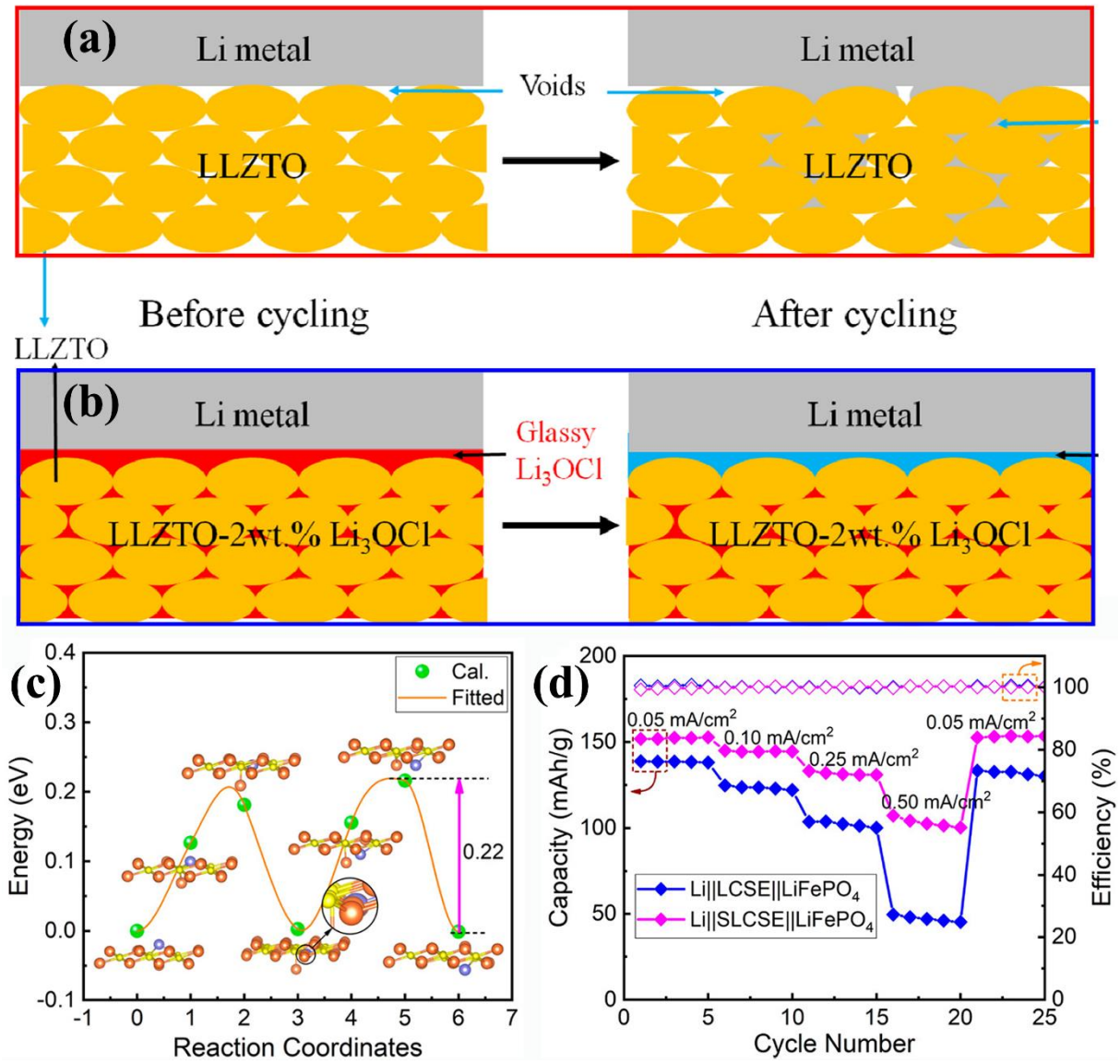

Fig. 13. Schematics of Li deposition behavior using (a) LLZTO particles solid-state electrolyte and (b) LLZTO-2wt.% Li_3OCl composite solid-state electrolyte, formation of the interfacial layer between LLZTO-2wt.% Li_3OCl and Li metal by in-situ reaction of Li_3OCl and Li metal.

(a, b) Reprinted with permission from Ref. [173]. Copyright 2018, Elsevier. (c) The migration energy barrier of Li ions passing through the Li_2S layer. (d) Rate performance of Li||LCSE||$LiFePO_4$ and Li||SLCSE||$LiFePO_4$ cells at different current densities. (c, d) Reprinted with permission from Ref. [174]. Copyright 2020, ACS.

In addition to the channels for Li^+ transport and interface compatibility, factors, such as the concentration of vacancies, the chemical and electrochemical stability of electrode interfaces, the blocking mechanism of lithium dendrite growth and the mechanical properties of the disordered SSEs, are critically important for improving the overall performance of LIBs. McGrogan et al. determined the mechanical properties of the disordered Li_2S-P_2S_5 SSE, including Young's modulus, hardness and fracture toughness [177,178]. They found that the low stiffness of Li_2S-P_2S_5 facilitated the accommodation of elastic mismatch with adjacent phases. Gao et al. prepared a $75Li_2S$-$15P_2S_5$-$10B_2S_3$ SSE through a ball-milling and then melt-quenching method [4]. Utilizing non-lithiophilic boron species as blocks could inhibit the formation and growth of lithium dendrites, resulting in the prolongation of all-solid-stated LIB lifetimes. More importantly, the authors confirmed the chemical and structural heterogeneity of the interface between SSEs and lithium metal anode by systematic characterization, and proposed a "multi-layer mosaic like" interface structure model. The findings are instructive for the subsequent development of SSEs with strong dendrite inhibition and ultra-long cycling life.

As mentioned above, it is believed that DMs, especially disordered organic materials, have great potential in improving the interface compatibility between SSE and electrode materials. Organic materials offer the advantages of flexible structural and functional design [179,180]. Designing lithophilic functional groups on organic SSEs may be a feasible strategy to reduce the interfacial impedance between SSEs and electrode materials, thereby enhancing the electrochemical performance of all-solid-state batteries. Unlike crystalline materials with rigid characteristics, many disordered organic materials exhibit plasticity. Therefore, organic SSEs can be in "soft contact" with electrode materials, thus reducing the interfacial impedance [181,182]. Notably, the anisotropic and open network structural features of DMs allow for enhancing Li^+ ion conduction in SSEs [183].

Wang et al. developed superior MOF glass-based SSEs for stable all-solid-state lithium–oxygen batteries [6]. Specifically, the MOF glass referred to the zinc-based ZIF-62 glass. These SSEs effectively inhibited dendrite growth and showcased long-term Li stripping/plating stability, resulting in high Li^+ conductivity (5×10^{-4} S cm^{-1} at 20 °C), a high Li^+ transference number (0.86), and improved electrochemical stability. They found that the deposition behavior of discharge products at the solid-solid interface can be effectively regulated by the ion/electron mixed-conducting cathode, which was fabricated using MOF glass and electronically

conductive polymers. Moreover, Ding et al developed solid-state polyethylene oxide electrolytes by applying a MOF glass (i.e., zinc-based ZIF-62 glass) as an isotropic functional filler [184]. They found that adding MOF glass reduced the T_g of the polymer phase, thus improving the mobility of the polymer chains, and thereby facilitating lithium-ion transport. The Li–lithium iron phosphate full batteries, which was constructed using the obtained electrolyte feature high cycle stability and rate capability. MOF glass displays great application potential in energy storage systems with good safety and high energy density.

3.4 Disordered coating layers

During the first charge/discharge cycle of LIBs, the electrolyte decomposition at the anode-electrolyte interface leads to the formation of a coating layer, namely a solid electrolyte interface (SEI), on the electrodes. This layer can protect the electrodes from electrolyte corrosion and guide the uniform Li^+ deposition/stripping [185,186]. The ideal SEI layer should also be homogeneous, facilitating Li^+ transfer. However, the in-situ formed SEI is usually fragile and grows unevenly, thereby inducing dendrite growth. Therefore, a homogeneous and robust artificial SEI layer, which can act as a dendrite barrier allowing for longer operation of LIBs, is urgently needed [187]. DM layers, showing a macroscopically homogeneous structure, high compositional flexibility, and no grain boundaries, could be good candidates for the formation of artificial SEI layers.

For the Si anode, the volume expansion occurs during the alloy/de-alloying reaction with lithium, leading to the anode collapse and hence, to irreversible capacity loss of the LIBs [188]. Li et al. prepared an artificial disordered SEI on the Si anode, which consisted of an inner layer of polydopamine and an outer layer of SEI film [189]. They demonstrated the capability of artificial disordered SEI in protecting Si crystal clusters from volume expansion. Dou et al. put disordered TiO_2 and graphene coatings onto the Si anode. They found that the maximum volume expansion of the composite anode was only 53% of that of the pure Si anode [190].

Apart from the protective function against volume changes of electrodes, the disordered coating layer can also facilitate uniform Li deposition and enhance Li^+ transport. In addition to its protective function against volume changes in electrodes, the disordered coating layer can also facilitate uniform Li deposition and enhance Li^+ transport. Xie et al. applied an electroplating method to deposit a disordered carbon nanocoating on the surface of a garnet-type SSE surface [191]. As illustrated in Fig. 14a, for the pure porous SSEs, lithium was deposited preferentially on the surface of SSE rather than on the internal pores (Figs. 14a1 and a2). In contrast, the lithium deposition was observed simultaneously on both the surface and internal pores of disordered carbon-coated SSEs (Figs. 14b, b1, and b2). Moreover, both the

initial and post-cycle impedance values of the disordered carbon-coated electrolyte were significantly lower than those of pure SSEs (Figs. 14cd). Therefore, the disordered carbon coating strategy can not only improve the ionic conductivity of the electrolyte but also promote the uniform deposition of lithium metal. Yoon et al. proposed a 'coating-plus-infusion' strategy whereby the cobalt boride (Co_xB) metallic glass was coated onto the surface and infused into grain boundaries (GBs) of $LiNi_{0.8}Co_{0.1}Mn_{0.1}O_2$ (NCM) [192], (Figs. 14e, f, f1, and f2). The addition of Co_xB metal glass enhanced the electronic conductivity of NCM and suppressed the side reactions between the electrode and the electrolyte. Therefore, the Co_xB-NCM composite cathode delivered a much better rate performance than the pure NCM cathode (Fig. 14g).

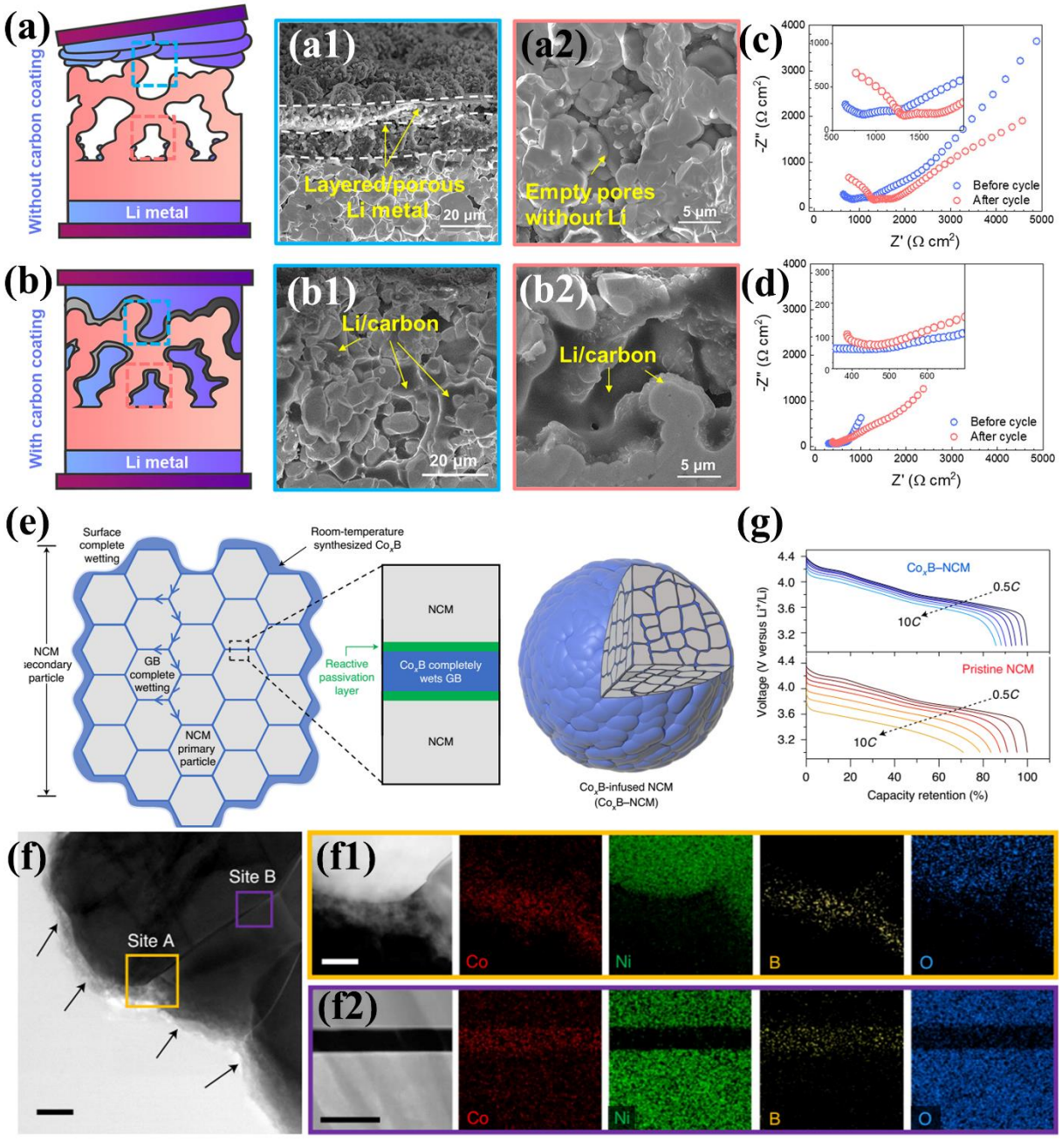

Fig. 14. Schematics to show the Li deposition (a) without or (b) with disordered carbon coating after cycling. SEM images to show local morphologies at the porous garnet electrolyte side (a1, a2) without or (b1, b2) with disordered carbon. EISs before and after cycling at room temperature of the solid-state Li-S battery in trilayer garnet (c) without or (d) with disordered carbon in the anode. (a-d) Reprinted with permission from Ref. [191]. Copyright 2021, ACS. (e) Schematic coating-plus-infusion microstructure in which Co_xB uniformly coats the surface of NCM secondary particles and infuses into GBs between the NCM primary particles. (f) TEM image of cross-sectioned Co_xB-NCM near the surface. EDS mappings of site A (f1) and site B (f2) in k. (g) Discharge curves at different rates for Co_xB-NCM (top) and pristine NCM (bottom). (e-g) Reprinted with permission from Ref. [192]. Copyright 2021, Nature.

Although significant progress has been made in the development of disordered coating layer materials on the electrodes and other components in LIBs [193,194], there are still many unresolved issues. These include determining if the coating is completely encapsulated on the surface of the target material, ensuring the uniformly distributed composition and optimal thickness of the coating. Reaching a consensus on these issues is essential for enhancing the efficacy of coating layer materials in LIBs.

3.5 Approaches for investigating Li ion storage and transfer mechanisms

The lithium charging/discharging process in disordered materials is accompanied by their microstructural evolutions, e.g., structural ordering. It is crucial to probe the microstructural evolution in disordered electrode materials during cycling and thereby reveal the mechanism of Li-ions storage and transfer. Yet, it is a great challenge to accurately detect and quantify this microstructural evolution. Nevertheless, recent years have witnessed notable advancements in understanding the lithium discharging/charging mechanisms within disordered electrode materials as described above. Some of the most effective methods are outlined here.

First, various in-situ/operando testing techniques, including X-ray diffraction, Neutron diffraction, XPS, Raman, X-ray absorption spectroscopy and synchrotron radiation, prove effective in detecting the changes of the local structure and chemical state of disordered materials throughout cycling processes. For example, operando pair distribution function analysis (PDF) and X-ray absorption spectroscopy were utilized to elucidate the structural evolution of the order-disorder transition and shed new light on the Cr-migration in the disordered state, which is the cause of the irreversibility of the Na-ion storage [195]. *Second*, PDF data derived from total X-ray scattering data can unveil alterations in the local atomic structure of disordered electrode materials throughout cycling, as demonstrated in [16]. This elucidation helps clarify the substantial enhancement observed in the Li-ion storage capacity during cycling. *Third*, solid-state nuclear magnetic resonance (NMR) stands as another potent technique capable of detecting local structural changes within disordered electrode materials.

This method also reveals the Li-ion storage mechanism and provides insights into Li-ion transfer kinetics within disordered materials, as reported in [15]. *Fourth*, theoretical calculations and simulations can contribute to clarifying the ion storage mechanism and ion transfer kinetics. Density functional theory (DFT) calculations are helpful for revealing Li/Na ion storage and transfer mechanisms, as well as redox reactions within the disorder electrode materials. Molecular dynamics (MD) simulations can provide insights into the dynamic behavior of disordered electrode materials during charge/discharge cycles. *Fifth*, the machine learning-based structural descriptor termed "softness" can be used as an indicator for both fracture resistance and ionic conductivity within glassy electrolytes as reported in [178].

4. Summary and Perspectives

Compared with the crystalline materials applied in LIBs, disordered materials have exhibited great promise owing to their many advantages, such as compositional flexibility, disordered open structure, structural stability, and redox reaction efficiency. This review demonstrated a range of research efforts focusing on synthesizing and applying novel DMs across various roles within LIBs, encompassing their use as cathodes, anodes, solid-state electrolytes, and protective layers.

After reviewing the application of DMs in LIBs, it becomes evident that these materials offer distinct advantages over their crystalline counterparts in four crucial aspects:

(1) *Li^+ storage advantage*. The open network structure of DMs used as anode materials can provide more storage sites for Li^+, thus improving the Li^+ storage capacity of anode materials. In addition, since the composition of DMs can be easily tuned, redox reactions can be tailored to enhance the Li^+ storage capacity of cathode materials.

(2) *Li^+ transport advantage*. DMs with open network structures and isotropic characteristics can provide a large number of transport channels for Li^+ transport in terms of number and direction, thus exhibiting excellent Li^+ transport performance. The Li^+ transport advantage of DMs is extremely attractive for cathode, anode, SSE, and coating layer materials.

(3) *Volume change-buffering advantage*. DMs with loose structures can maintain electrochemical activity even when subjected to repeated and substantial volume changes resulting from Li^+ insertion/extraction. This aspect holds particular significance for both anode and cathode materials.

(4) *High structural reversibility*. DMs generally exhibit excellent structural reversibility since they do not have a periodic atomic arrangement and thus do not undergo any irreversible structural transformation of crystalline materials (e.g., the order-to-disorder transition during

Li^+ insertion/extraction). Therefore, the strategy of amorphization can avoid the irreversible phase transition, which occurs in some cathode materials (e.g., V_2O_5) during Li^+ insertion/extraction. It should be mentioned that the accumulation of energy during deep charging/discharging may lead to the appearance of a transition from disorder to order.

While DMs exhibit numerous fascinating features in connection to LIBs, more in-depth and refined studies are needed to expand our understanding of the disorder-performance relationship of LIBs so that superior LIBs can be developed. To further enhance DM performance in LIBs, future investigations should prioritize consideration of these four key aspects:

(1) *The microscopic mechanism of the disorder-induced enhancement of the LIB performances*. There is a necessity to establish universal laws governing such mechanisms.

(2) *The flexibility of the component adjustment in DMs*. This advantage should be further utilized to design redox reaction pairs with higher reaction potentials and to achieve a larger number of these pairs for disordered inorganic cathode materials.

(3) *Rational structural design and characterizations*. According to the storage mode of Li^+ in disordered anode materials, the lithium storage spaces (such as holes and vacancies, as well as Li^+ transport channels) can be designed by tuning atomic structures through precise composition adjustment. More advanced testing techniques should be developed for in-situ observation of the structural evolution in DMs during Li^+ insertion/extraction. Thus, the derived structural information will be used to optimize the DMs for superior LIBs.

(4) *Seeking solutions for interface problems*. Interfacial issues are a significant challenge in the development of SSEs and coating layer materials. Disordered organic SSEs and coating materials are expected to lower the interfacial impedance caused by the rigid contact between conventional SSEs and electrodes since these materials are mechanically deformable. Under this premise, the big question is how we can achieve optimum compatibility and higher ionic conductivity in the interface between SSEs and electrodes. This question must be answered by the future investigation.

(5) *Structural heterogeneity in DMs.* It is recognized that inherent structural heterogeneity characterizes both melt-quenched glasses and other DMs [196-198], serving as a precursor to nano-phase separation and nano-crystallization. Thus, it can be deduced that structural heterogeneity could benefit the disorder-to-order transition frequently observed in DMs during charging/discharging cycles within LIBs. Moreover, the degree of structural heterogeneity varies among different DM systems. Therefore, it is important to investigate the impact of structural heterogeneity in DMs on the electrochemical performance of LIBs. Such an

investigation could contribute to a rational design of DMs, particularly melt-quenched glasses, towards achieving enhanced performance in LIBs.

In this review article, we have outlined the promising potential of DMs in the development of advanced LIBs for diverse applications. Additionally, we have shed light on the influence of structural disorder on electrochemical performances of LIBs. However, there remain unresolved challenges in enhancing both the electrochemical and mechanical characteristics of DMs. Addressing these issues, we foresee that a collaborative effort among scientists and technologists across various scientific disciplines will lead to further breakthroughs.

Acknowledgements

This work was supported by the Liaocheng University Ph.D. Start-up Foundation (318052012). Z. Du thanked the funding support from China Scholarship Council/University College London for the joint Ph.D. scholarship. Y. Zhang would like to acknowledge the support of the Taishan Youth Scholar Project of Shandong Province (tsqn202103098), the Natural Science Foundation of Shandong Province (ZR2020ME025) and the Colleges and Universities New Twenty Terms Foundation of Jinan City (No. 202333073).

References

[1] S.T. Han, P. Wen, H.J. Wang, Y. Zhou, Y. Gu, L. Zhang, Y.S.-Horn, X.R. Lin, M. Chen, Sequencing polymers to enable solid-state lithium batteries, Nat. Mater. 2023. https://doi.org/10.1038/s41563-023-01693-z.

[2] Z.Y. Wang, Z.J. Du, Y.Y. Liu, C.E. Knapp, Y.H. Dai, J.W. Li, W. Zhang, R.W. Chen, F. Guo, W. Zong, X. Gao, J.X. Zhu, C.L. Wei, G.J. He, Metal-organic frameworks and their derivatives for optimizing lithium metal anodes, eScience 2023. https://doi.org/10.1016/j.esci.2023.100189.

[3] W. Zhang, Y.H. Dai, R.W. Chen, Z.M. Xu, J.W. Li, W. Zong, H.X. Li, Z. Li, Z.Y. Zhang, J.X. Zhu, F. Guo, X. Gao, Z.J. Du, J.T. Chen, T.L. Wang, G.J. He, I.P. Parkin, Highly reversible zinc metal anode in a dilute aqueous electrolyte enabled by a pH buffer additive, Angew. Chem. Int. Ed. 62 (2023) e202212695. https://doi.org/10.1002/anie.202212695.

[4] C.W. Gao, J.H. Zhang, C.M. He, Y.Q. Fu, T.Y. Zhou, X. Li, S.L. Kang, L.L. Tan, Q. Jiao, S.X. Dai, Y.Z. Yue, C.G. Lin, Unveiling the growth mechanism of the interphase between lithium metal and Li_2S-P_2S_5-B_2S_3 solid-state electrolytes, Adv. Energy Mater. 13 (2023) 2204386. https://doi.org/10.1002/ aenm.202204386.

[5] R.W. Chen, C.Y. Zhang, J.W. Li, Z.J. Du, F. Guo, W. Zhang, Y.H. Dai, W. Zong, X. Gao, J.X. Zhu, Y. Zhao, X.H. Wang, G.J. He, A hydrated deep eutectic electrolyte with finely-tuned solvation chemistry for high-performance zinc-ion batteries, Energy Environ. Sci. 16 (2023) 2540-2549. https://doi.org/10.1039 /d3ee00462g

[6] X.X. Wang, D.H. Guan, C.L. Miao, J.X. Li, J.Y. Li, X.Y. Yuan, X.Y. Ma, J.J. Xu, Boundary-free metal-organic framework glasses enable highly stable all-solid-state

lithium-oxygen battery, Adv. Energy Mater. (2023) 2303829. https://doi.org/10.1002/aenm.202303829.
[7] S.Q. Li, K. Wang, G.F. Zhang, S. Li, Y.N. Xu, X.D. Zhang, X. Zhang, S.H. Zheng, X.Z. Sun, Y.W. Ma, Fast charging anode materials for lithium-ion batteries: current status and perspectives, Adv. Funct. Mater. 32 (2022) 2200796. https://doi.org/10.1002/adfm.202200796.
[8] J. Neumann, M. Petranikova, M. Meeus, J.D. Gamarra, R. Younesi, M. Winter, S. Nowak, Recycling of lithium-ion batteries-current state of the art, circular economy, and next generation recycling, Adv. Energy Mater. 12 (2022) 2102917. https://doi.org/10.1002/aenm.202102917.
[9] J.L. Yang, X.X. Zhao, W.H. Li, H.J. Liang, Z.Y. Gu, Y. Liu, M. Du, X.L. Wu, Advanced cathode for dual-ion batteries: waste-to-wealth reuse of spent graphite from lithium-ion batteries, eScience 2 (2022) 95-101. https://doi.org/10.1016/j.esci.2021.11.001.
[10] F.Y. Xiong, Q.Y. An, L. Xia, Y. Zhao, L.Q. Mai, H.Z, Tao, Y.Z. Yue, Revealing the atomistic origin of the disorder-enhanced Na-storage performance in $NaFePO_4$ battery cathode, Nano Energy 57 (2019) 608-615. https://doi.org/10.1016/j.nanoen.2018.12.087.
[11] Y.F. Zhang, P.X. Wang, T. Zheng, D.M. Li, G.D. Li, Y.Z. Yue, Enhancing Li-ion battery anode performances via disorder/order engineering, Nano Energy 49 (2018) 596-602. https://doi.org/10.1016 /j.nanoen.2018.05.018.
[12] Y.F. Zhang, P.X. Wang, G.D. Li, J.H. Fan, C.W. Gao, Z.Y. Wang, Y.Z. Yue, Clarifying the charging induced nucleation in glass anode of Li-ion batteries and its enhanced performances, Nano Energy 57 (2019) 592-599. https://doi.org/10.1016/j.nanoen.2018.12.088.
[13] C.W. Gao, P.X. Wang, Z.Y. Wang, S.K. Kær, Y.F. Zhang, Y.Z. Yue, The disordering-enhanced performances of the Al-MOF/graphene composite anodes for lithium ion batteries, Nano Energy 65 (2019) 104032. https://doi.org/10.1016/j.nanoen.2019.104032.
[14] J.J. Yan, C.W. Gao, S.B. Qi, Z.J. Jiang, L.R. Jensen, H.B. Zhan, Y.F. Zhang, Y.Z. Yue, Encapsulation of nano-Si into MOF glass to enhance lithium-ion battery anode performances, Nano Energy 103 (2022) 107779. https://doi.org/10.1016/j.nanoen.2022.107779.
[15] Z.J. Jiang, T.Y. Zhao, J.J. Ren, Y.F. Zhang, Y.Z. Yue, NMR evidence for the charge-discharge induced structural evolution in a Li-ion battery glass anode and its impact on the electrochemical performances, Nano Energy 80 (2021) 105589. https://doi.org/10.1016/j.nanoen.2020.105589.
[16] C.W. Gao, Z.J. Jiang, S.B. Qi, P.X. Wang, L.R. Jensen, M. Johansen, C.K. Christensen, Y.F. Zhang, D.B. Ravnsbæk, Y.Z. Yue, Metal-organic framework glass anode with an exceptional cycling-induced capacity enhancement for lithium-ion batteries, Adv. Mater. 34 (2022) 2110048. https://doi.org/ 10.1002/adma.202110048.
[17] S.B. Qi, X.Y. Li, Z.J. Jiang, J.Y. Zhang, Z.T. Shan, Y.F. Zhang, Enhancing glass anode performance for lithium-ion batteries via crystallization, J. Am. Ceram. Soc. 105 (2022) 1001-1009. https://dor.org/10.1111/jace.18165.
[18] S.B Qi, X.Y. Li, Y.Z. Yue, Y.F. Zhang, Iron phosphate glass-ceramic anodes for lithium ion batteries, Int. J. Appl. Glass Sci. 13 (2022) 420-428. https://doi.org/10.1111/ijag.16557.
[19] X.B. Su, Y.C. Li, J.Y. Zhang, Z.T. Shan, Y.F. Zhang, Phosphosilicate glass anode for fast charging lithium-ion batteries, Mater. Lett. 354 (2024) 135422. https://doi.org/10.1016/j.matlet.2023.135422.
[20] C.K. Christensen, D.B. Ravnsbæk, Understanding disorder in oxide-based electrode materials for rechargeable batteries, J. Phys. Energy 3 (2021) 031002. https://doi.org/10.1088/2515-7655/abf0f1.
[21] S.S. Zhang, Z.H. Li, K. Luo, J.L. He, Y.F. Gao, A.V. Soldatov, V. Benavides, K.Y. Shi, A.M. Nie, B. Zhang, W.T. Hu, M.D. Ma, Y. Liu, B. Wen, G.Y. Gao, B. Liu, Y. Zhang, Y.

Shu, D.L. Yu, X.F. Zhou, Z.S. Zhao, B. Xu, L. Su, G.Q. Yang, O.P. Chernogorova, Y.J. Tian, Discovery of carbon-based strongest and hardest amorphous material, Natl. Sci. Rev. 9 (2022) nwab140. https://doi.org/10.1093/nsr/nwab140.
[22] Y.Z. Yue, The hardest amorphous material, Natl. Sci. Rev. 9 (2022) nwab203. https://doi.org/10.1093 /nsr/nwab203.
[23] Z.H. Li, Y.J. Wang, M.D. Ma, H.C. Ma, W.T. Hu, X. Zhang, Z.W. Zhuge, S.S. Zhang, K. Luo, Y.F. Gao, L. Sun, A.V. Soldatov, Y.J. Wu, B. Liu, B.Z. Li, P. Ying, Y. Zhang, B. Xu, J.L. He, D.L. Yu, Z.Y. Liu, Z.S. Zhao, Y.Z. Yue, Y.J. Tian, X.Y. Li, Ultrastrong conductive in situ composite composed of nanodiamond incoherently embedded in disordered multilayer graphene. Nat. Mater. 22 (2023) 42–49. https://doi.org/10.1038/s41563-022-01425-9.
[24] M.A. Ali, W.M.W. Winters, M.A. Mohamed, D.Z. Tan, G.J. Zheng, R.S.K. Madsen, O.V. Magdysyuk, M. Diaz-Lopez, B. Cai, N. Gong, Y.J. Xu, I. Hung, Z.H. Gan, S. Sen, H.-T. Sun, T.D. Bennett, X.F. Liu, Y.Z. Yue, J.R. Qiu, Fabrication of super-sized metal inorganic-organic hybrid glass with supramolecular network via crystallization-suppressing approach. Angew. Chem. Int. Ed. 62 (2023) e202218094. https://doi.org/10.1002/ange.202218094.
[25] R.S.K. Madsen, A. Qiao, J. Sen, I. Hung, K.Z. Chen, Z.H. Gan, S. Sen, Y.Z. Yue, Ultrahigh-field ^{67}Zn NMR reveals short-range disorder in zeolitic imidazolate framwork glasses, Science 367 (2020) 1473-1476. https://doi.org/10.1126/science.aaz0251.
[26] C. Jung, S.J. Kim, J. Jang, J.H. Ko, D. Kim, B. Ko, Y.M. Song, S.H. Hong, J. Rho, Disordered-nanoparticle-based etalon for ultrafast humidity-responsive colorimetric sensors and anti-counterfeiting displays, Sci. Adv. 8 (2022) eabm8598. https://doi.org/10.1126/sciadv.abm859.
[27] J.W. Ding, D.F. Ji, Y.Z. Yue, M.M. Smedskjaer, Amorphous materials for lithium-ion and post-lithium-ion batteries, Small 2023. https://doi.org/10.1002/smll.202304270.
[28] T. Bernges, R. Hanus, B. Wankmiller, K. Imasato, S.Q. Lin, M. Ghidiu, M. Gerlitz, M. Peterlechner, S. Graham, G. Hautier, Y.Z. Pei, M.R. Hansen, G. Wilde, G.J. Snyder, J. George, M.T. Agne, W.G. Zeier, Considering the role of ion transport in diffuson-dominated thermal conductivity, Adv. Energy Mater. 12 (2022) 2200717. https://doi.org/10.1002/aenm.202200717.
[29] J.H. Ku, J.H. Ryu, S.H. Kim, O.H. Han, S.M. Oh, Reversible lithium storage with high mobility at structural defects in amorphous molybdenum dioxide electrode, Adv. Funct. Mater. 22 (2012) 3658-3664. https://doi.org/10.1002/adfm.201102669.
[30] J.T. Ding, T. Fan, K. Shen, Y.W. Li, Electrochemical synthesis of amorphous metal hydroxide microarrays with rich defects from MOFs for efficient electrocatalytic water oxidation, Appl. Catal. B: Environ. 292 (2021) 120174. https://doi.org/10.1016/j.apcatb.2021.120174.
[31] W.F. Zhai, T. Sakthivel, F.Y. Chen, C.F. Du, H. Yu, Z.F. Dai, Amorphous materials for elementary-gas-involved electrocatalysis: an overview, Nanoscale 13 (2021) 19783-19811. https://doi.org/10.1039 /D1NR06764H.
[32] V.N. Thuc, H.A. Tam, D.T.H. Giang, N.H. Duc, N.T. Ngoc, V.T.N. Khanh, L.V. Lich, V.-H. Dinh, Hierarchical geometric designs for Fe-based amorphous materials with tunable soft magnetic properties, J. Alloys Compd. 895 (2022) 162628. https://doi.org/10.1016/j.jallcom.2021.162628.
[33] Y.J. Ma, G.W. Xiao, X.Y. Fang, T.H. Chen, D.P. Yan, Leveraging crystalline and amorphous states of a metal-organic complex for transformation of the photosalient effect and positive-negative photochromism, Angew. Chem. Int. Ed. 135 (2023) e202217054. https://doi.org/10.1002 /ange.202217054.

[34] S. Afyon, F. Krumeich, C. Mensing, A. Borgschulte, R. Nesper, New high capacity cathode materials for rechargeable Li-ion batteries: vanadate-borate glasses, Sci. Rep. 4 (2014) 7113. https://doi.org/ 10.1038/srep07113.
[35] N. Abid, A.M. Khan, S. Shujait, K. Chaudhary, M. Ikram, M. Imran, J. Haider, M. Khan, Q. Khan, M. Maqbool, Synthesis of nanomaterials using various top-down and bottom-up approaches, influencing factors, advantages, and disadvantages: a review, Adv. Colloid Interface. Sci. 300 (2022) 102597. https://doi.org/10.1016/j.cis.2021.102597.
[36] H.F. Tian, Y.H. Ma, Z.J. Li, M.Y. Cheng, S.C. Ning, E.X. Han, M.Q. Xu, P.F. Zhang, K.X. Zhao, R.J. Li, Y.Y. Zou, P.C. Liao, S.L. Yu, X.M. Li, J.L. Wang, S.Z. Liu, Y.F. Li, X.Y. Huang, Z.X. Yao, D.D. Ding, J.G. Guo, Y. Huang, J.M. Lu, Y.Y. Han, Z. Wang, Z.G. Cheng, J. Liu, Z. Xu, K. Liu, P. Gao, Y. Jiang, L. Lin, X. Zhao, L. Wang, X. Bai, W. Fu, J.Y. Wang, M. Li, T. Lei, Y. Zhang, Y. Hou, J. Pei, S.J. Pennycook, E. Wang, J. Chen, W. Zhou, L. Liu, Disorder-tuned conductivity in amorphous monolayer carbon, Nature 615 (2023) 56-61. http://doi.org/10.1038/s41586-022-05617-w.
[37] H.W. Zhao, X.J. Chen, G.Z. Wang, Y.F. Qiu, L. Guo, Two-dimensional amorphous nanomaterials: synthesis and applications, 2D Mater. 6 (2019) 032002. http://doi.org/10.1088/2053-1583/ab1169.
[38] M.J.V. Vleet, T.T. Weng, X.Y. Li, J.R. Schmidt, In situ, time-resolved, and mechanistic studies of metal–organic framework nucleation and growth, Chem. Rev. 118 (2018) 3681-3721. https://doi.org/ 10.1021/acs.chemrev.7b00582.
[39] T.D. Bennett, A.K. Cheetham, Amorphous metal-organic frameworks, Acc. Chem. Res. 47 (2014) 1555-1562. https://doi.org/10.1021/ar5000314.
[40] M.W. Yuan, R. Wang, Z.M. Sun, L. Lin, H. Yang, H.F. Li, C.Y. Nan, G.B. Sun, S.L. Ma, Morphology-controlled synthesis of Ni-MOFs with highly enhanced electrocatalytic performance for urea oxidation, Inorg. Chem. 58 (2019) 11449-11457. https://doi.org/10.1021/acs.inorgchem.9b01124.
[41] V. Subramaniyam, D.T. Thangadurai, P.V. Ravi, M. Pichumani, Do the acid/base modifiers in solvothermal synthetic conditions influence the formation of Zr-Tyr MOFs to be amorphous?, J. Mol. Struct. 1267 (2022) 133611. https://doi.org/10.1016/j.molstruc.2022.133611.
[42] F. Zhao, W.X. Yang, Y. Han, X.L. Luo, W.Z. Tang, T.L. Yue, Z.H. Li, A straightforward strategy to synthesize supramolecular amorphous zirconium metal-organic gel for efficient Pb(II) removal, Chem. Eng. J. 407 (2021) 126744. https://doi.org/10.1016/j.cej.2020.126744.
[43] Q. Ouyang, G.S. Li, X.Q. Liu, Q. Wang, X. Zhang, J.X. Wang, Z.P. Fan, G.C. Gao, L.P. Li, Chemically interconnected amorphous nanospheres SiO_xC_y as high performance anodes, Electrochim. Acta 426 (2022) 140772. https://doi.org/10.1016/j.electacta.2022.140772.
[44] B.H. An, D.M. Xu, R. Geng, Y. Cheng, R.B. Qian, X.C. Tang, Z.Q. Fan, H.B. Chen, The pretreatment effects of various target pollutant in real coal gasification gray water by coupling pulse electrocoagulation with chemical precipitation methods, Chemosphere 311 (2023) 136898. https://doi. org/10.1016/j.chemosphere.2022.136898.
[45] B.B. Jia, R. Hao, Z.N. Huang, P.F. Hu, L.D. Li, Y. Zhang, L. Guo, Creating ultrathin amorphous metal hydroxide and oxide nanosheet libraries, J. Mater. Chem. A 7 (2019) 4383-4388. https://doi.org/ 10.1016/10.1039/C8TA11525G.
[46] J.R. Esquius, D.J. Morgan, G.A. Siller, D. Gianolio, M. Aramini, L. Lahn, O. Kasian, S.A. Kondrat, R. Schlögl, G.J. Hutchings, R. Arrigo, S.J. Freakley, Lithium-directed transformation of amorphous iridium (oxy)hydroxides to produce active water oxidation catalysts, J. Am. Chem. Soc. 145 (2023) 6398-6409. https://doi.org/10.1021/jacs.2c13567.
[47] H.D. Li, H.Y. Li, Y.Z. Lai, Z.W. Yang, Q. Yang, Y. Liu, Z. Zheng, Y.X. Liu, Y. Sun, B.H. Zhong, Z.G. Wu, X.D. Guo, Revisiting the preparation progress of nano-structured Si

anodes toward industrial application from the perspective of cost and scalability, Adv. Energy Mater. 12 (2022) 2102181. https:// doi.org/10.1002/aenm.202102181.
[48] Y. Yang, G. Yoon, S. Park, S.D. Namgung, T. Badloe, K.T. Nam, J. Rho, Revealing structural disorder in hydrogenated amorphous silicon for a low-loss photonic platform at visible frequencies, Adv. Mater. 33 (2021) e2005893. https://doi.org/10.1002/adma.202005893.
[49] B. Gupta, M.A. Hossain, A. Riaz, A. Sharma, D.D. Zhang, H.H. Tan, C. Jagadish, K. Catchpole, B. Hoex, S. Karuturi, Recent advances in materials design using atomic layer deposition for energy applications, Adv. Funct. Mater. 32 (2021) 2109105. https://doi.org/10.1002/adfm.202109105.
[50] A. Meena, P. Thangavel, D.S. Jeong, A.N. Singh, A. Jana, H. Im, D.A. Nguyen, K.S. Kim, Crystalline-amorphous interface of mesoporous Ni_2P@$FePO_xH_y$ for oxygen evolution at high current density in alkaline-anion-exchange-membrane water-electrolyzer, Appl. Catal. B: Environ. 306 (2022) 121127. https://doi.org/10.1016/j.apcatb.2022.121127.
[51] M.Y. Gao, J.R. Zeng, Q.B. Zhang, C. Yang, X.T. Li, Y.X. Hua, C.Y. Xu, Scalable one-step electrochemical deposition of nanoporous amorphous S-doped $NiFe_2O_4$/Ni_3Fe composite films as highly efficient electrocatalysts for oxygen evolution with ultrahigh stability, J. Mater. Chem. A 6 (2018) 1551-1560. https://doi.org/10.1039/C7TA08474A.
[52] B. Sarac, T. Karazehir, M. Micusik, C. Halkali, D. Gutnik, M. Omastova, A.S. Sarac, J. Eckert, Origin of electrocatalytic activity in amorphous nickel-metalloid electrodeposits, ACS Appl. Mater. Interfaces 13 (2021) 23689-23701. https://doi.org/10.1021/acsami.1c03007.
[53] Y.B. Xu, H.P. Wu, H. Jia, J.G. Zhang, W. Xu, C.M. Wang, Current density regulated atomic to nanoscale process on Li deposition and solid electrolyte interphase revealed by cryogenic transmission electron microscopy, ACS Nano 14 (2020) 8766-8775. https://doi.org/10.1021/acsnano.0c03344.
[54] Z.T. Shan, T.Y. Zhao, X.F. Ke, J.J. Ren, H.Z. Tao, Y.Z. Yue, Oxygen tri-clusters make glass highly crack-resistant, Acta. Mater. 2024. https://doi.org/10.1016/j.actamat.2023.119425.
[55] Z.J. Du, A. Qiao, H.M. Zhou, Z.C. Li, W.M.W. Winters, J.X. Zhu, G.J. He, I.P. Parkin, H.Z. Tao, Y.Z. Yue, The glass transition in the high-density amorphous Zn/Co-ZIF-4, Chem. Commun. 59 (2023) 11871-11874. https://doi.org/10.1039/D3CC02492J.
[56] F.Y. Xu, G. Nava, P. Biswas, I. Dulalia, H.Y. Wang, Z. Alibay, M. Gale, D.J. Kline, B. Wagner, L. Mangolini, M.R. Zachariah, Energetic characteristics of hydrogenated amorphous silicon nanoparticles, Chem. Eng. J. 430 (2022) 133140. https://doi.org/10.1016/j.cej.2021.133140.
[57] A.S. Westover, A.K. Kercher, M. Kornbluth, M. Naguib, M.J. Palmer, D.A. Cullen, N.J. Dudney, Plasma synthesis of spherical crystalline and amorphous electrolyte nanopowders for solid-state batteries, ACS Appl. Mater. Interfaces 12 (2020) 11570-11578. https://doi.org/10.1021/acsami.9b20812.
[58] Z.Y. Wu, G.Y. Gao, J.B. Zhang, A. Soldatov, J. Kim, L. Wang, Y.J. Tian, Tunable electrical properties of C_{60}·m-xylene and the formation of semiconducting ordered amorphous carbon clusters under pressure, Nano Res. 15 (2022) 3788-3793. https://doi.org/10.1007/s12274-022-4092-1.
[59] C. Wu, S.Q. Yang, Y. Li, Y.F. Ma, L. Zhang, J.J. Liu, S.M. Han, Microstructural evolution and electrochemical properties of the ultra-high pressure treated $La_{0.7}Mg_{0.3}Ni_{3.3}$ hydrogen storage alloy, J. Alloys Compd. 665 (2016) 231-239. https://doi.org/10.1016/j.jallcom.2016.01.039.
[60] D.W. Zhang, P. Schoenherr, P. Sharma, J. Seidel, Ferroelectric order in van der Waals layered materials, Nat. Rev. Mater. 8 (2022) 25-40. https://doi.org/10.1038/s41578-022-00484-3.

[61] R.R. Petersen, J.F.S. Christensen, N.T. Jørgensen, S. Gustafson, L.A. Lindbjerg, Y.Z. Yue, Preparation and thermal properties of commercial vermiculite bonded with potassium silicate, Thermochim. Acta 699 (2021) 178926. https://doi.org/10.1016/j.tca.2021.178926.
[62] R.R. Petersen, M.B. Olesen, J. König, Y.Z. Yue, Expansion and shrinkage of lightweight vermiculite material at high temperatures, Ceram. Int. 49 (2023) 23605-23611. https://doi.org/10.1016/j.ceramint. 2023.04.195.
[63] H. Kaur, B. Konkena, C. Gabbett, R. Smith, M. McCrystall, R.Y. Tian, A. Roy, T. Carey, V. Vega-Mayoral, V. Nicolosi, J.N. Coleman, Amorphous 2D-nanoplatelets of red phosphorus obtained by liquid-phase exfoliation yield high areal capacity Na-ion battery anodes, Adv. Energy Mater. 13 (2022) 2203013. https://doi.org/10.1002/aenm.202203013.
[64] L.H. Jin, R.S. Guo, T. Han, R.B. Wang, Y. Zhang, Ultrathin 2D violet phosphorus nanosheets: facile liquid-phase exfoliation, characterization, and photoelectrochemical application, Adv. Funct. Mater. 33 (2023) 2213583. https://doi.org/10.1002/adfm.202213583.
[65] M. Fujioka, M. Jeem, K. Sato, M. Tanaka, K. Morita, T. Shibuya, K. Takahashi, S. Iwasaki, A. Miura, M. Nagao, S. Demura, H. Sakata, M. Ono, H. Kaiju, J. Nishii, Intercalation on transition metal trichalcogenides via a quasi-amorphous phase with 1D order, Adv. Funct. Mater. 33 (2023) 2208702. https://doi.org/10.1002/adfm.202208702.
[66] C. Deng, Y.X. Gao, Y.B. Yao, B. Liang, S.G. Lu, T. Tao, Conversion of layered materials to ultrathin amorphous nanosheets induced by ball-milling insertion and pure-water exfoliation, J. Mater. Chem. A 10 (2022) 11766-11773. https://doi.org/10.1039/D2TA02237K.
[67] Q.J. Zheng, Y.F. Zhang, M. Montazerian, O. Gulbiten, J. C. Mauro, E. D. Zanotto, Y.Z. Yue, Understanding glass through differential scanning calorimetry, Chem. Rev. 119 (2019) 7848-7939. https://doi.org/10.1021/acs.chemrev.8b00510.
[68] N. Li, J.H. Peng, P. Zhang, Y.Z. Yue, Amorphous MXene opens new perspectives, Adv. Mater. 35 (2023) 2300067. https://doi.org/10.1002/adma.202300067.
[69] A. Qiao, H.Z. Tao, Y.Z. Yue, Enhancing ionic conductivity in Ag_3PS_4 via mechanical amorphization, J. Non-Cryst. Solids 521 (2019) 119476. https://doi.org/10.1016/j.jnoncrysol.2019.119476.
[70] J. Kim, Y. Kim, J. Yoo, G. Kwon, Y. Ko, K. Kang, Organic batteries for a greener rechargeable world, Nat. Rev. Mater. 8 (2022) 54-70. https://doi.org/10.1038/s41578-022-00478-1.
[71] S.B. Zheng, D.J. Shi, T.J. Sun, L.T. Zhang, W.J. Zhang, Y.X. Li, Z.B. Guo, Z.L. Tao, J. Chen, Hydrogen bond networks stabilized high-capacity organic cathode for lithium-ion, Angew. Chem. Int. Ed. 62 (2023) e202217710. https://doi.org/10.1002/ange.202217710.
[72] P.F. Sang, Q.L. Chen, D.Y. Wang, W. Guo, Y.Z. Fu, Organosulfur materials for rechargeable batteries: structure, mechanism, and application, Chem. Rev. 123 (2023) 1262-1326. https://doi.org/10.1021/acs. chemrev.2c00739.
[73] Y.W. Zheng, H.Q. Ji, J. Liu, Z.K Wang, J.Q. Zhou, T. Qian, C.L. Yan, Surpassing the redox potential limit of organic cathode materials via extended p-π conjugation of dioxin, Nano Lett. 22 (2022) 3473-3479. https://doi.org/10.1021/acs.nanolett.2c00965.
[74] T.Y. Zhu, H. Sternlicht, Y. Ha, C. Fang, D.Y. Liu, B.H. Savitzky, X. Zhao, Y.Y. Lu, Y.B. Fu, C. Ophus, C.H. Zhu, W.L. Yang, A.M. Minor, G. Liu, Formation of hierarchically ordered structures in conductive polymers to enhance the performances of lithium-ion batteries, Nat. Energy, 8 (2023) 129-137. https://doi.org/10.1038/s41560-022-01176-6.
[75] Z. Yang, T. Wang, H. Chen, X. Suo, P. Halstenberg, H. Lyu, W. Jiang, S.M. Mahurin, I. Popovs, S. Dai, Surpassing the organic cathode performance for lithium-ion batteries with robust fluorinated covalent quinazoline networks, ACS Energy Lett. 6 (2020) 41-51. https://doi.org/10.1021/acsenergylett.0c01750.

[76] A. Molina, N. Patil, E. Ventosa, M. Liras, J. Palma, R. Marcilla, New anthraquinone-based conjugated microporous polymer cathode with ultrahigh specific surface area for high-performance lithium-ion batteries, Adv. Funct. Mater. 30 (2019) 1908074. https://doi.org/10.1002/adfm.201908074.
[77] Y. Zheng, T. Qian, H. Ji, X. Xia, J. Liu, Y. Zhu, C. Yan, Accelerating ion dynamics under cryogenic conditions by the amorphization of crystalline cathodes, Adv. Mater. 33 (2021) e2102634. https://doi. org/10.1002/adma.202102634.
[78] J.Z. Sheng, Q.D. Li, Q.L. Wei, P.F. Zhang, Q.Q. Wang, F. Lv, Q.Y. An, W. Chen, L.Q. Mai, Metastable amorphous chromium-vanadium oxide nanoparticles with superior performance as a new lithium battery cathode, Nano Res. 7 (2014) 1604-1612. https://doi.org/10.1007/s12274-014-0520-1.
[79] M. Kindle, Y. Cha, J.S. McCloy, M.K. Song, Alternatives to cobalt: vanadate glass and glass-ceramic structures as cathode materials for rechargeable lithium-ion batteries, ACS Sustainable Chem. Eng. 9 (2021) 629-638. https://doi.org/10.1021/acssuschemeng.0c04026.
[80] X. Zhang, X.h. Sun, X. Li, X.D. Hu, S. Cai, C.M. Zheng, Recent progress in rate and cycling performance modifications of vanadium oxides cathode for lithium-ion batteries, J. Energy Chem. 59 (2021) 343-363. https://doi.org/10.1016/j.jechem.2020.11.022.
[81] C.K. Christensen, D.R. Sørensen, J. Hvam, D.B. Ravnsbæk, Structural evolution of disordered $Li_xV_2O_5$ bronzes in V_2O_5 cathodes for Li-ion batteries, Chem. Mater. 31 (2019) 512-520. https://10.1021/acs.chemmater.8b04558.
[82] M. Xie, X. Sun, H.T. Sun, T. Porcelli, S.M. George, Y. Zhou, J. Lian, Stabilizing an amorphous V_2O_5/carbon nanotube paper electrode with conformal TiO_2 coating by atomic layer deposition for lithium ion batteries, J. Mater. Chem. A 4 (2016) 537-544. https://doi.org/10.1039/C5TA01949D.
[83] F. Mattelaer, K. Geryl, G. Rampelberg, J. Dendooven, C. Detavernier, Amorphous and crystalline vanadium oxides as high-energy and high-power cathodes for three-dimensional thin-film lithium ion batteries, ACS Appl. Mater. Interfaces 9 (2017) 13121-13131. https://doi.org/10.1021/acsami.6b16473.
[84] M.Y. Du, K.K. Huang, Y.M. Guo, Z.W. Xie, H. Jiang, C.J. Li, Y.J. Chen, High specific capacity lithium ion battery cathode material prepared by synthesizing vanadate-phosphate glass in reducing atmosphere, J. Power Sources 424 (2019) 91-99. https://doi.org/10.1016/j.jpowsour.2019.03.106.
[85] F.H. Kong, D. Wang, X.W. Cheng, M.H. Li, C.J. Li, Multi-electron reactions and chain conversion of amorphous cathodes to improve the specific capacity of rechargeable lithium batteries, J. Non-Cryst. Solids 599 (2023) 121985. https://doi.org/10.1016/j.jnoncrysol.2022.121985.
[86] F.H. Kong, X. Liang, L.L. Yi, X.H. Fang, Z.B. Yin, Y.L. Wang, R.X. Zhang, L.Y. Liu, Q. Chen, M.H. Li, C.J. Li, H. Jiang, Y.J. Chen, Multi-electron reactions for the synthesis of a vanadium-based amorphous material as lithium-ion battery cathode with high specific capacity, Energy 219 (2021) 119513. https://doi.org/10.1016/j.energy.2020.119513.
[87] F.H. Kong, D. Sun, Y.Z. Rao, R.X. Zhang, Z.L. Chen, D. Wang, X.L. Yu, H. Jiang, C.J. Li, Order-disorder transition in amorphous vanadium-phosphorus-lithium cathode of lithium ion battery, Appl. Surf. Sci. 573 (2022) 151490. https://doi.org/10.1016/j.apsusc.2021.151490.
[88] F.H. Kong, L.L. Yi, S.J. Huang, X. Liang, Y.Z. Rao, Z.Q. Su, C.J. Li, H. Jiang, Using glass defect engineering to obtain order–disorder transformation in cathode for high specific capacity lithium ion battery, Appl. Surf. Sci. 552 (2021) 149495. https://doi.org/10.1016/j.apsusc.2021.149495.

[89] R. Thirupathi, V. Kumari, S. Chakrabarty, S. Omar, Recent progress and prospects of NASICON framework electrodes for Na-ion batteries, Prog. Mater. Sci. 137 (2023) 101128. https://doi.org/10. 1016/j.pmatsci.2023.101128.
[90] D. Bin, Y.Y. Du, B.B. Yang, H.B. Lu, Y. Liu, Y.Y. Xia, Progress of phosphate-based polyanion cathodes for aqueous rechargeable zinc batteries, Adv. Funct. Mater. 33 (2022) 2211765. https://doi.org/10.1002/ adfm.202211765.
[91] P. Hu, T. Zhu, C.C. Cai, X.P. Wang, L. Zhang, L.Q. Mai, L. Zhou, A high-energy NASICON-type $Na_{3.2}MnTi_{0.8}V_{0.2}PO_{4.3}$ cathode material with reversible 3.2-electron redox reaction for sodium-ion batteries, Angew. Chem. Int. Edit. 135 (2023) e202219304. https://doi.org/10.1002/ange.202219304.
[92] L. Yue, J.Y. Zhang, M. Kong, K. Li, W.H. Zhang, X.T. Guo, M.M. Xiao, F. Zhang, H. Pang, Watermelon-like multicore-shell $Fe(PO_3)_2$@carbon nanocapsule anode to construct an all iron phosphate-based sodium ion battery, Nano Res. 15 (2022) 9026-9037. https://doi.org/10.1007/s12274-022-4678-7.
[93] T.C. Liu, Y.C. Feng, Y.D. Duan, S.H. Cui, L.P. Lin, J.T. Hu, H. Guo, Z.Q. Zhuo, J.X. Zheng, Y. Lin, W.L. Yang, K. Amine, F. Pan, Formation of mono/bi-layer iron phosphate and nucleation of $LiFePO_4$ nano-crystals from amorphous 2D sheets in charge/discharge process for cathode in high-performance Li-ion batteries, Nano Energy 18 (2015) 187-195. https://doi.org/10.1016/j.nanoen.2015.10.016.
[94] Y.S. Hong, K.S. Ryu, Y.J. Park, M.G. Kim, J.M. Lee, S.H. Chang, Amorphous $FePO_4$ as 3 V cathode material for lithium secondary batteries, J. Mater. Chem. 12 (2002) 1870-1874. https://doi.org/10.1039/ B200901C.
[95] Z.Y. Wang, Y.C. Lu, Facile construction of high-performance amorphous $FePO_4$/carbon nanomaterials as cathodes of lithium-ion batteries, ACS Appl. Mater. Interfaces 11 (2019) 13225-13233. https://doi. org/10.1021/acsami.8b22720.
[96] T.B. Zhang, X.B. Cheng, Q. Zhang, Y.C. Lu, G.S. Luo, Construction of a cathode using amorphous $FePO_4$ nanoparticles for a high-power/energy-density lithium-ion battery with long-term stability, J. Power Sources 324 (2016) 52-60. https://doi.org/10.1016/j.jpowsour.2016.05.071.
[97] R.W. Mo, D. Rooney, K.N. Sun, J.N. Wang, 3D holey-graphene frameworks cross-linked with encapsulated mesoporous amorphous $FePO_4$ nanoparticles for high-power lithium-ion batteries, Chem. Eng. J. 417 (2021) 128475. https://doi.org/10.1016/j.cej.2021.128475.
[98] S. Okada, T. Yamamoto, Y. Okazaki, J. Yamaki, M. Tokunaga, T. Nishida, Cathode properties of amorphous and crystalline $FePO_4$, J. Power Sources 146 (2005) 570-574. https://doi.org/10.1016/ j.jpowsour.2005.03.200.
[99] Y. Sabi, S. Sato, S. Hayashi, T. Furuya, S. Kusanagi, A new class of amorphous cathode active material $Li_xM_yPO_z$ (M=Ni, Cu, Co, Mn, Au, Ag, Pd), J. Power Sources 258 (2014) 54-60. https://doi.org/ 10.1016/j.jpowsour.2014.02.021.
[100] A. Kitajou, Y. Ishado, A. Inoishi, S. Okada, Amorphous $xLiF\text{-}FeSO_4$ ($1 \leq x \leq 2$) composites as a cathode material for lithium ion batteries, Solid State Ionics 326 (2018) 48-51. https://doi.org/10.1016/ j.ssi.2018.09.007.
[101] S. Pazhaniswamy, A.K. Parameswaran, N. Balakrishnan, S. Goel, Z. Sofer, S.K. Yadav, C.S. Panneerselvam, Prediction clue on the fading capacity of multi-walled carbon nanotube-decorated $Li_2(Fe_{1-x}Ti_x)SiO_4$/C high-performance cathode materials, Energy Fuel. 35 (2021) 8321-8333. https://doi. org/10.1021/acs.energyfuels.1c00269.
[102] A. Mitra, S. Jena, S.B. Majumder, S. Das, Supercapacitor like behavior in nano-sized, amorphous mixed poly-anion cathode materials for high power density lithium and other alkali-metal ion batteries, Electrochim. Acta 338 (2020) 135899. https://doi.org/10.1016/j.electacta.2020.135899.
[103] L. Su, J.K. Ren, T. Lu, K.X. Chen, J.W. Ouyang, Y. Zhang, X.Y. Zhu, L.Y. Wang, H.H. Min, W. Luo, Z.F. Sun, Q.B. Zhang, Y. Wu, L.T. Sun, L.Q. Mai, F. Xu, Deciphering

structural origins of highly reversible lithium storage in high entropy oxides with in situ transmission electron microscopy, Adv. Mater. 35 (2023) e2205751. https://doi.org/10.1002/adma.202205751.
[104] Y.L. Huang, B.W. Shao, Y. Wang, F.D. Han, Solid-state silicon anode with extremely high initial coulombic efficiency, Energy Environ. Sci. 16 (2023) 1569-1580. https://doi.org/10.1039/D2EE04057C.
[105] Y. Xin, S. Pan, X.Z. Hu, C. Miao, S.Q. Nie, H.Y. Mou, W. Xiao, Engineering amorphous SnO_2 nanoparticles integrated into porous N-doped carbon matrix as high-performance anode for lithium-ion batteries, J. Colloid Interface Sci. 639 (2023) 133-144. https://doi.org/10.1016/j.jcis.2023.02.065.
[106] Y.H. Tang, J.J. Chen, Z.Y. Mao, C. Roth, D.J. Wang, Highly N-doped carbon with low graphitic-N content as anode material for enhanced initial coulombic efficiency of lithium-ion batteries, Carbon Energy 5 (2022) e257. https://doi.org/10.1002/cey2.257.
[107] C.J. Xu, L. Shen, W.J. Zhang, Y.L. Huang, Z.F. Sun, G.Y. Zhao, Y.B. Lin, Q.B. Zhang, Z.G. Huang, J.X. Li, Efficient implementation of kilogram-scale, high-capacity and long-life Si-C/TiO_2 anodes, Energy Storage Mater. 56 (2023) 319-330. https://doi.org/10.1016/j.ensm.2023.01.025.
[108] X.Y. Chen, J.Y. Tian, P. Li, Y.L. Fang, Y.J. Fang, X.M. Liang, J.W. Feng, J. Dong, X.P. Ai, H.X. Yang, Y.L. Cao, An overall understanding of sodium storage behaviors in hard carbons by an "adsorption-intercalation/filling"hybrid mechanism, Adv. Energy Mater. 12 (2022) 2200886. https://doi. org/10.1002/aenm.202200886.
[109] J.F. Lin, W.Q. Song, C.X. Xiao, J.N. Ding, Z.C. Huang, C. Zhong, J. Ding, W.B. Hu, A comprehensive overview of the electrochemical mechanisms in emerging alkali metal–carbon dioxide batteries, Carbon Energy 5 (2023) e313. https://doi.org/10.1002/cey2.313.
[110] Y. Lechón, C. Lago, I. Herrera, A.R. Gamarra, A. Pérula, Carbon benefits of different energy storage alternative end uses. Application to the Spanish case, Renew. Sust. Energy Rev. 171 (2023) 112985. https://doi.org/10.1016/j.rser.2022.112985.
[111] W.H. Liang, Y.K. Tang, L. Liu, Y. Gao, X.Y. Zeng, Physical forces inducing thin amorphous carbon nanotubes derived from polymer nanotube/SiO_2 hybrids with superior rate capability for lithium-ion batteries, ACS Appl. Mater. Interfaces 11 (2019) 36985-36990. https://doi.org/10.1021/acsami.9b13207.
[112] Y.X. Wang, W. Tian, L.H. Wang, H.R. Zhang, J.L. Liu, T.Y. Peng, L. Pan, X.B. Wang, M.B. Wu, A tunable molten-salt route for scalable synthesis of ultrathin amorphous carbon nanosheets as high-performance anode materials for lithium-ion batteries, ACS Appl. Mater. Interfaces 10 (2018) 5577-5585. https://doi.org/10.1021/acsami.7b18313.
[113] X. Li, S.J. Zhang, J. Du, L.L. Liu, C. Mao, J. Sun, A.B. Chen, Strong interaction between phosphorus and wrinkle carbon sphere promote the performance of phosphorus anode material for lithium-ion batteries, Nano Res. 16 (2023) 9273-9279. https://doi.org/10.1007/s12274-023-5499-z.
[114] M.R. Su, J.L. Li, K.D. He, K. Fu, P. Nui, Y.C. Chen, Y. Zhou, A.C. Dou, X.C. Hou, Y.J. Liu, NiSb/nitrogen-doped carbon derived from Ni-based framework as advanced anode for lithium-ion batteries, J. Colloid Interface Sci. 629 (2023) 83-91. https://doi.org/10.1016/j.jcis.2022.08.126.
[115] G.J. Yang, X.Y. Li, Z. Guan, Y.X. Tong, B. Xu, X.F. Wang, Z.X. Wang, L.Q. Chen, Insights into lithium and sodium storage in porous carbon, Nano Lett. 20 (2020) 3836-3843. https://doi.org/10.1021/ acs.nanolett.0c00943.
[116] D. Li, M. Zhang, L.X. Zhang, X.Q. Xu, Q.C. Pan, Y.G. Huang, F.H. Zheng, H.Q. Wang, Q.Y. Li, Constructing three-dimensional N-doped carbon coating silicon/iron silicide nanoparticles cross-linked by carbon nanotubes as advanced anode materials for lithium-ion batteries, J. Colloid Interface Sci. 629 (2022) 908-916. https://doi.org/10.1016/j.jcis.2022.09.143.

[117] Y.H. Lu, Z.T. Ye, Y.T. Zhao, Q. Li, M.Y. He, C.C. Bai, X.T. Wang, Y.L. Han, X.C. Wan, S.L. Zhang, Y.F. Ma, Y. Chen, Graphene supported double-layer carbon encapsulated silicon for high-performance lithium-ion battery anode materials, Carbon 201 (2023) 962-971. https://doi.org/10.1016/j.carbon. 2022.10.010.
[118] Y. Chu, J. Zhang, Y.B. Zhang, Q. Li, Y.R. Jia, X.M. Dong, J. Xiao, Y. Tao, Q.H. Yang, Reconfiguring hard carbons with emerging sodium-ion batteries: a perspective, Adv. Mater. 35 (2023) 2212186. https: doi.org/10.1002/adma.202212186.
[119] X.W. Dou, I. Hasa, D. Saurel, C. Vaalma, L.M. Wu, D. Buchholz, D. Bresser, S. Komaba, S. Passerini, Hard carbons for sodium-ion batteries: structure, analysis, sustainability, and electrochemistry, Mater. Today 23 (2019) 87-104. https://doi.org/10.1016/j.mattod.2018.12.040.
[120] C.C. Cai, Y.A. Chen, P. Hu, T. Zhu, X.Y. Li, Q. Yu, L. Zhou, X.Y. Yang, L.Q. Mai, Regulating the interlayer spacings of hard carbon nanofibers enables enhanced pore filling sodium storage, Small 18 (2022) 2105303. https://doi.org/10.1002/smll.202105303.
[121] R. Chen, X.Y. Li, C.C. Cai, H. Fan, Y.J. Deng, H.G. Yu, L.Q. Mai, L. Zhou, Amine-aldehyde condensation-derived N-doped hard carbon microspheres for high-capacity and robust sodium storage, Small 19 (2023) 2303790. https://doi.org/10.1002/smll.202303790.
[122] H.W. Chen, Y.D. Lu, H.J. Zhu, Y.C. Guo, R. Hu, R. Khatoon, L.X. Chen, Y.J. Zeng, L. Jiao, J.X. Leng, J.G. Lu, Crystalline SnO_2@amorphous TiO_2 core-shell nanostructures for high-performance lithium ion batteries, Electrochim. Acta 310 (2019) 203-212. https://doi.org/10.1016/j.electacta.2019.04.134.
[123] N. Makivić, J.Y. Cho, K.D. Harris, J.M. Tarascon, B. Limoges, V. Balland, Evidence of bulk proton insertion in nanostructured anatase and amorphous TiO_2 electrodes, Chem. Mater. 33 (2021) 3436-3448. https://doi.org/10.1021/acs.chemmater.1c00840.
[124] Y. Liu, C.F. Ding, X.D. Yan, P.T. Xie, B.Q. Xu, L.L. Chen, Y.C. Liu, C.Z. Liu, Y.H. Yu, Y.H. Lin, Interface-strain-confined synthesis of amorphous TiO_2 mesoporous nanosheets with stable pseudocapacitive lithium storage, Chem. Eng. J. 420 (2021) 129894. https://doi.org/10.1016/j.cej.2021. 129894.
[125] Y. Qi, X.Q. Zeng, L.P. Xiao, X.Y. Li, H.G. Liao, Q.C. Xu, J. Xu, An invisible hand: hydrogen bonding guided synthesis of ultrathin two-dimensional amorphous TiO_2 nanosheets, Sci. China Mater. 65 (2022) 3017-3024. https://doi.org/10.1007/s40843-022-2097-2.
[126] J.A. Yuwono, P. Burr, C. Galvin, A. Lennon, Atomistic insights into lithium storage mechanisms in anatase, rutile, and amorphous TiO_2 electrodes, ACS Appl. Mater. Interfaces 13 (2021) 1791-1806. https://doi.org/10.1021/acsami.0c17097.
[127] P. Xue, C. Sun, H.P. Li, J.J. Liang, C. Lai, Superlithiophilic Amorphous SiO_2-TiO_2 distributed into porous carbon skeleton enabling uniform lithium deposition for stable lithium metal batteries, Adv. Sci. 6 (2019) 1900943. https://doi.org/10.1002/advs.201900943.
[128] H. Zhou, M. Alam, Y.C. Wu, Y. Zeng, A.N. Gandi, J.X. Zheng, W.J. Zhu, Z.C. Wang, H.F. Liang, Synergy of VN and Fe_2O_3 enables high performance anodes for asymmetric supercapacitors, ACS Appl. Mater. Interfaces 15 (2023) 18819-18827. https://doi.org/10.1021/acsami.2c22848.
[129] Q.S. Zhao, J.L. Liu, X.X. Li, Z.Z. Xia, Q.X. Zhang, M. Zhou, W. Tian, M. Wang, H. Hu, Z.T. Li, W.T. Wu, H. Ning, M.B. Wu, Graphene oxide-induced synthesis of button-shaped amorphous Fe_2O_3/rGO/CNFs films as flexible anode for high-performance lithium-ion batteries, Chem. Eng. J. 369 (2019) 215-222. https://doi.org/10.1016/j.cej.2019.03.076.
[130] Z.M. Qin, Y. Song, Y.Z. Liu, X.X. Liu, Aqueous calcium-ion storage in amorphous molybdenum oxide, Chem. Eng. J. 451 (2023) 138681. https://doi.org/10.1016/j.cej.2022.138681.

[131] P.F. Yan, L. Ji, X.P. Liu, Q.H. Guan, J.L. Guo, Y.L. Shen, H.J. Zhang, W.F. Wei, X.W. Cui, Q. Xu, 2D amorphous-MoO_{3-x}@Ti_3C_2-MXene non-van der Waals heterostructures as anode materials for lithium-ion batteries, Nano Energy 86 (2021) 106139. https://doi.org/10.1016/j.nanoen.2021.106139.
[132] H.Y. Wu, S.Q. Zhou, C.H. Tseng, M.L. Qin, A. Shiue, A. Chu, Z.Q. Cao, B. Jia, X.H. Qu, One-pot solution combustion synthesis of crystalline and amorphous molybdenum trioxide as anode for lithium-ion battery, J. Am. Ceram. Soc. 104 (2020) 1102-1109. https://doi.org/10.1111/jace.17499.
[133] J. Kjeldsen, A.C.M. Rodrigues, S. Mossin, Y.Z. Yue, Critical V_2O_5/TeO_2 ratio inducing abrupt property changes in vanadium tellurite glasses, J. Phys. Chem. B 118 (2014) 14942−14948. https://doi.org/10.1021/jp508910m.
[134] J. Kjeldsen, Y.Z. Yue, C.B. Bragatto, A.C.M. Rodrigues, Electronic conductivity of vanadium-tellurite glass-ceramics, J. Non-Cryst. Solids 378 (2013) 196-200. https://doi.org/10.1016/j.jnoncrysol.2013.07.011.
[135] S.Li, A. Qiao, C.W. Gao, Y.F. Zhang, Y.L. Yue, Y.Z. Yue, Mechanical and dynamic properties of V_2O_5-TeO_2-P_2O_5 glasses. J. Alloy Comp. 863 (2021) 158074. https://doi.org/10.1016/j.jallcom.2020.158074.
[136] J.H. Fan, Y.F. Zhang, G.D. Li, Y.Z. Yue, Tellurium nanoparticles enhanced electrochemical performances of TeO_2-V_2O_5-Al_2O_3 glass anode for lithium-ion batteries, J. Non-Cryst. Solids 521 (2019) 119491. https://doi.org/10.1016/j.jnoncrysol.2019.119491.
[137] Z.J. Jiang, S.B. Qi, C.W. Gao, X.Y. Li, Y.F. Zhang, Y.Z. Yue, Water enables a performance jump of glass anode for lithium-ion batteries, J. Non-Cryst. Solids 576 (2022) 121225. https://doi.org/10.1016/ j.jnoncrysol.2021.121225.
[138] J.J. Yan, T.T. Zhao, N. Shi, H.B. Zhan, J.J. Ren, Y.F. Zhang, Y.Z. Yue, Impact of silicon doping on the structure and crystallization of a vanadium-tellurite glass, J. Non-Cryst. Solids 589 (2022) 121651. https://doi.org/10.1016/j.jnoncrysol.2022.121651.
[139] X.Y. Li, P.W. Li, X. Liu, S.H. Luo, Y.C. Li, X.B. Su, Y.Z. Zhang, Y.Z. Yue, Grid-like Fe_3O_4 nanocrystals enhance the performances of glass-ceramic anodes for lithium-ion batteries, J. Non-Cryst. Solids 605 (2023) 122157. https://doi.org/10.1016/j.jnoncrysol.2023.122157.
[140] T.Y. Zhao, Z.J. Jiang, Y.F. Zhang, J.J. Ren, Y.Z. Yue, V_2O_5-P_2O_5-TeO_2 glass anodes for Li-ion batteries, J. Non-Cryst. Solids 600 (2023) 122014. https://doi.org/10.1016/j.jnoncrysol.2022.122014.
[141] S.B. Qi, X.Y. Li, Y.Z. Yue, Y.F. Zhang, Iron-phosphate glass-ceramic anodes for lithium-ion batteries, Int. J. Appl. Glass Sci. 13 (2022) 420-428. https://doi.org/10.1111/ijag.16557.
[142] F.Y. Xiong, H.Z. Tao, Y.Z. Yue, Role of amorphous phases in enhancing performances of electrode materials for alkali ion batteries. Front. Mater. 6 (2020) 328. https://doi.org/10.3389/fmats.2019.00328.
[143] Y.F. zhang, Glass anodes for lithium ion batteries: Insight from the structural evolution during discharging/charging, Int J Appl Glass Sci. 11 (2020) 577–589. https://doi.org/10.1111/ijag.15079.
[144] W. He, X.D. Zhang, C. Jin, Y.Y. Wang, S. Mossin, Y.Z. Yue, Nano-glass ceramic cathodes for Li^+/Na^+ mixed-ion batteries, J. Power Sources 342 (2017) 717-725. https://doi.org/10.1016/j.jpowsour. 2016.12.118.
[145] A. Qiao, T.D. Bennett, H.Z. Tao, A. Krajnc, G. Mali, C.M. Doherty, A.W. Thornton, J.C. Mauro, G.N. Greaves, Y.Z. Yue, A metal-organic framework with ultrahigh glass-forming ability, Sci. Adv. 4 (2018) eaao6827. https://doi.org/10.1126/sciadv.aao6827.
[146] Z.M. Zheng, H.H. Wu, H.D. Liu, Q.B. Zhang, X. He, S.C. Yu, V. Petrova, J. Feng, R. Kostecki, P. Liu, D.L. Peng, M. Liu, M.S. Wang, Achieving fast and durable lithium storage through amorphous FeP nanoparticles encapsulated in ultrathin 3D P-doped

porous carbon nanosheets, ACS Nano 14 (2020) 9545-9561. https://doi.org/10.1021/acsnano.9b08575.
[147] W.W. Li, J.L. Yu, J.J. Wen, J. Liao, Z.Y. Ye, B.T. Zhao, X.W. Li, H.Y. Zhang, M.L. Liu, Z.P. Guo, An amorphous Zn–P/graphite composite with chemical bonding for ultra-reversible lithium storage, J. Mater. Chem. A 7 (2019) 16785-16792. https://doi.org/10.1039/C9TA01431D.
[148] R.R. Ding, J.Z. Zhang, J. Zhang, Z.H. Li, C.Y. Wang, M.M. Chen, Core-shell Fe_2N@amorphous carbon nanocomposite-filled 3D graphene framework: an additive-free anode material for lithium-ion batteries, Chem. Eng. J. 360 (2019) 1063-1070. https://doi.org/10.1016/j.cej.2018.10.177.
[149] G.D. Park, J.K. Lee, Y.C. Kang, Electrochemical reaction mechanism of amorphous iron selenite with ultrahigh rate and excellent cyclic stability performance as new anode material for lithium-ion batteries, Chem. Eng. J. 389 (2020) 124350. https://doi.org/10.1016/j.cej.2020.124350.
[150] S.X. Mei, B. Xiang, S.G. Guo, J.G. Deng, J.J. Fu, X.M. Zhang, Y. Zheng, B. Gao, K. Huo, P.K. Chu, Design and electrochemical mechanism of the MgF_2 coating as a highly stable and conductive interlayer on the Si anode for high-performance Li-ion batteries, Adv. Funct. Mater. (2023) 2301217. https://doi.org/10.1002/adfm.202301217.
[151] A.K. Prajapati, A. Bhatnagar, A review on anode materials for lithium/sodium-ion batteries, J. Energy Chem. 83 (2023) 509-540. https://doi.org/10.1016/j.jechem.2023.04.043.
[152] G. Kim, S.Y. Jeong, J.H. Shin, J. Cho, H. Lee, 3D amorphous silicon on nanopillar copper electrodes as anodes for high-rate litihum-ion batteries, ACS Nano 8 (2014) 1907-1912. https://doi.org/10.1021/ nn406464c.
[153] M. Salah, C. Hall, C. Francis, G.R. Walker, M. Fabretto, Binary silicon-based thin-film anodes for lithium-ion batteries: a review, J. Power Sources 520 (2022) 230871. https://doi.org/10.1016/j.jpowsour. 2021.230871.
[154] L.F. Cui, R. Ruffo, C.K. Chen, H.L. Peng, Y. Cui, Crystalline-amorphous core-shell silicon nanowires for high capacity and high current battery electrodes, Nano Lett. 9 (2009) 491-495. https://doi.org/10. 1021/nl8036323.
[155] A.Y. Su, J. Li, J.J. Dong, D. Yang, G. Chen, Y.J. Wei, An amorphous/crystalline incorporated Si/SiO_x anode material derived from biomass corn leaves for lithium-ion batteries, Small 16 (2020) e2001714. https://doi.org/10.1002/smll.202001714.
[156] F. Wang, X.B. Liao, H.Y. Wang, Y. Zhao, J. Mao, D.G. Truhlar, Bioinspired mechanically interlocking holey graphene@SiO_2 anode, Interdiscip. Mater. 1 (2022) 517-525. http://doi.org/10.1002/idm2.12032.
[157] Z.H. Liu, D.D. Guan, Q. Yu, L. Xu, Z.C. Zhuang, T. Zhu, D.Y. Zhao, L. Zhou, L.Q. Mai, Monodisperse and homogeneous SiOx/C microspheres: A promising high-capacity and durable anode matrials for lithium-ion batteries, Energy Storage Mater. 13 (2018) 112-118. https://doi.org/10.1016/j.ensm.2018.01.004.
[158] Z.H. Liu, Y.L. Zhao, R.H. He, W. Luo, J.S. Meng, Q. Yu, D.Y. Zhao, L. Zhou, L.Q. Mai, Yolk@shell SiOx/C microspheres with semi-graphitic carbon coating on the exterior and interior surfaces for durable lithium storage, Energy Storage Mater. 19 (2019) 299-305. https://doi.org/10.1016/j.ensm.2018.10.011.
[159] P.U. Nzereogu, A.D. Omah, F.I. Ezema, E.I. Iwuoha, A.C. Nwanya, Anode materials for lithium-ion batteries: a review, Appl. Surf. Sci. Adv. 9 (2022) 100233. https://doi.org/10.1016/j.apsadv.2022. 100233.
[160] K. Stokes, H. Geaney, M. Sheehan, D. Borsa, K.M. Ryan, Copper silicide nanowires as hosts for amorphous Si deposition as a route to produce high capacity lithium-ion battery anodes, Nano Lett. 19 (2019) 8829-8835. https://doi.org/10.1021/acs.nanolett.9b03664.

[161] G. Lin, H. Wang, L. Zhang, Q. Cheng, Z. Gong, K. Ostrikov, Graphene nanowalls conformally coated with amorphous/ nanocrystalline Si as high-performance binder-free nanocomposite anode for lithium-ion batteries, J. Power Sources 437 (2019) 226909. https://doi.org/10.1016/j.jpowsour.2019.226909.
[162] Z.H. Wang, Y. Li, S.Z. Huang, L.X. Liu, Y. Wang, J. Jin, D.Z. Kong, L. Zhang, O.G. Schmidt, PVD customized 2D porous amorphous silicon nanoflakes percolated with carbon nanotubes for high areal capacity lithium ion batteries, J. Mater. Chem. A 8 (2020) 4836-4843. https://doi.org/10.1039/ C9TA12923E.
[163] S.Y. Yuan, K. Ding, X.Y. Zeng, D. Bin, Y.J. Zhang, P. Dong, Y.G. Wang, Advanced nonflammable organic electrolyte promises safer Li-metal batteries: from solvation structure perspectives, Adv. Mater. 35 (2023) e2206228. https://doi.org/10.1002/adma.202206228.
[164] Y.J. Xie, J.Y. Wang, B.H. Savizky, Z. Chen, Y. Wang, S. Betzler, K. Bustillo, K. Persson, Y. Cui, L.W. Wang, C. Ophus, P. Ercius, H.M. Zheng, Spatially resolved structural order in low-temperature liquid electrolyte, Sci. Adv. 9 (2023) eadc9721. https://doi.org/10.1126/sciadv.adc9721.
[165] Z. Li, R. Yu, S. Weng, Q.H. Zhang, X.F. Wang, X. Guo, Tailoring polymer electrolyte ionic conductivity for production of low- temperature operating quasi-all-solid-state lithium metal batteries, Nat. Commun., 14 (2023) 482. https://doi.org/10.1038/s41467-023-35857-x.
[166] S.L. Liu, W.Y. Liu, D.L. Ba, Y.Z. Zhao, Y.H. Ye, Y.Y. Li, J.P. Liu, Filler-integrated composite polymer electrolyte for solid-state lithium batteries, Adv. Mater. 35 (2023) e2110423. https://doi.org/ 10.1002/adma.202110423.
[167] T.T. Zuo, F. Walther, J.H. Teo, R. Rueß, Y.B. Wang, M. Rohnke, D. Schröder, L.F. Nazar, J. Janek, Impact of the chlorination of lithium argyrodites on the electrolyte/cathode interface in solid-state batteries, Angew. Chem. Int. Ed. 62 (2023) e202213228. https://doi.org/10.1002/anie.202213228.
[168] Y. Nikodimos, W.N. Su, B.J. Hwang, Halide solid-state electrolytes: stability and application for high voltage all-solid-state Li batteries, Adv. Energy Mater. 13 (2022) 2202854. https://doi.org/10.1002/ aenm.202202854
[169] S. Xue, Y.D. Liu, Y.P. Li, D. Teeters, D.W. Crunkleton, S.W. Wang, Diffusion of lithium ions in amorphous and crystalline poly(ethylene oxide)$_3$:$LiCF_3SO_3$ polymer electrolytes, Electrochim. Acta 235 (2017) 122-128. https://doi.org/10.1016/j.electacta.2017.03.083.
[170] Z.Y. Lin, X.W. Guo, H.J. Yu, Amorphous modified silyl-terminated 3D polymer electrolyte for high-performance lithium metal battery, Nano Energy 41 (2017) 646-653. https://doi.org/10.1016/j.nanoen. 2017.10.021.
[171] E.C. Self, Z.D. Hood, T. Brahmbhatt, F.M. Delnick, H.M. Meyer, G. Yang, J.L.M. Rupp, J. Nanda, Solvent-mediated synthesis of amorphous Li_3PS_4/polyethylene oxide composite solid electrolytes with high Li^+ conductivity, Chem. Mater. 32 (2020) 8789-8797. https://doi.org/10.1021/acs.chemmater. 0c01990.
[172] Z. Zhang, X. Wang, X. Li, J. Zhao, G. Liu, W. Yu, X. Dong, J. Wang, Review on composite solid electrolytes for solid-state lithium-ion batteries, Mater. Today Sustainability 21 (2023) 100316. https://doi.org/10.1016/j.mtsust.2023.100316.
[173] Y.J. Tian, F. Ding, H. Zhong, C. Liu, Y.B. He, J.Q. Liu, X.J. Liu, Q. Xu, $Li_{6.75}La_3Zr_{1.75}Ta_{0.25}O_{12}$@amorphous Li_3OCl composite electrolyte for solid state lithium-metal batteries, Energy Storage Mater. 14 (2018) 49-57. https://doi.org/10.1016/j.ensm.2018.02.015.
[174] C. Lai, C.Y. Shu, W. Li, L. Wang, X.W. Wang, T.R. Zhang, X.S. Yin, I. Ahmad, M.T. Li, X.L. Tian, P. Yang, W. Tang, N.H. Miao, G.W. Zheng, Stabilizing a lithium metal battery by an in situ Li_2S-modified interfacial layer via amorphous-sulfide composite solid electrolyte, Nano Lett. 20 (2020) 8273-8281. https://doi.org/10.1021/acs.nanolett.0c03395.

[175] R. Zhao, G.T. Hu, S. Kmiec, R. Gebhardt, A. Whale, J. Wheaton, S.W. Martin, New amorphous oxy-sulfide solid electrolyte material: anion exchange, electrochemical properties, and lithium dendrite suppression via in situ interfacial modification, ACS Appl. Mater. Interfaces 13 (2021) 26841-26852. https://doi.org/10.1021/acsami.0c22305.
[176] J.H. Wu, L. Shen, Z.H. Zhang, G.Z. Liu, Z.Y. Wang, D. Zhou, H.L. Wan, X.X. Xu, X.Y. Yao, All-solid-state lithium batteries with sulfide electrolytes and oxide cathodes, Electrochem. Energy Rev. 4 (2020) 101-135. https://doi.org/10.1007/s41918-020-00081-4.
[177] F.P. McGrogan, T. Swamy, S.R. Bishop, E. Eggleton, L. Porz, X.W. Chen, Y.M. Chiang, K.J.V. Vliet, Compliant yet brittle mechanical behavior of Li_2S–P_2S_5 lithium-ion-conducting solid electrolyte, Adv. Energy Mater. 7 (2017) 1602011. https://doi.org/10.1002/aenm.201602011.
[178] T. Du, Z.M. Chen, H. Liu, Q. Zhang, M. Bauchy, Y.Z. Yue, M.M. Smedskjaer, Controlling factor for fracture resistance and ionic conduction in glassy lithium borophosphate electrolytes, Mater. Today Energy 37 (2023) 101390. https://doi.org/10.1016/j.mtener.2023.101390.
[179] Y. Su, X. Rong, A. Gao, Y. Liu, J. Li, M. Mao, X. Qi, G. Chai, Q. Zhang, L. Suo, L. Gu, H. Li, X. Huang, L. Chen, B. Liu, Y.S. Hu, Rational design of a topological polymeric solid electrolyte for high-performance all-solid-state alkali metal batteries, Nat. Commun. 13 (2022) 4181. https://doi.org/10. 1038/s41467-022-31792-5.
[180] J. Pan, Y.C. Zhang, J. Wang, Z.C. Bai, R.G. Cao, N.N. Wang, S.X. Dou, F.Q. Huang, A quasi-double-layer solid electrolyte with adjustable interphases enabling high-voltage solid-state batteries, Adv. Mater. 34 (2022) e2107183. https://doi.org/10.1002/adma.202107183.
[181] J.Park, D.B. Ahn, J. Kim, E. Cha, B.S. Bae, S.Y. Lee, J.U. Park, Printing of wirelessly rechargeable solid-state supercapacitors for soft, smart contact lenses with continuous operations, Sci. Adv. 5 (2019) eaay0764. https://doi.org/10.1126/sciadv.aay076.
[182] O.B. Chae, B.L. Lucht, Interfacial issues and modification of solid electrolyte interphase for Li metal anode in liquid and solid electrolytes, Adv. Energy Mater. 13 (2023) 2203791. https://doi.org/10.1002/ aenm.202203791.
[183] A. Manthiram, X.W. Yu, S.F. Wang, Lithium battery chemistries enabled by solid-state electrolytes, Nat. Rev. Mater. 2 (2017) 16103. https://doi.org/10.1038/natrevmats.2016.103.
[184] J.W. Ding, T. Du, E.H. Thomsen, D. Andresen, M.R. Fischer, A.K. Møller, A.R. Petersen, A.K. Pedersen, L.R. Jensen, S.W. Wang, M.M. Smedskjaer, Metal-organic framework glass as a functional filler enables enhanced performance of solid-state polymer electrolytes for lithium metal batteries, Adv. Sci. (2023) 2306698. https://doi.org/10.1002/advs.202306698.
[185] M.Y. Yang, S.V. Zybin, T. Das, B.V. Merinov, W.A. Goddard, E.K. Mok, H.J. Hah, H.E. Han, Y.C. Choi, S.H. Kim, Characterization of the solid electrolyte interphase at the Li metal–ionic liquid interface, Adv. Energy Mater. 13 (2022) 2202949. https://doi.org/10.1002/aenm.202202949.
[186] H. Adenusi, G.A. Chass, S. Passerini, K.V. Tian, G. Chen, Lithium batteries and the solid electrolyte interphase (SEI)-progress and outlook, Adv. Energy Mater. 13 (2023) 2203307. https://doi.org/10. 1002/aenm.202203307.
[187] Z. Yang, M.X. Jiang, C. Cui, Y.X. Wang, J.W. Qin, J. Wang, Y. Wang, B.G. Mao, M.H. Cao, In-situ cross-linking strategy for stabilizing the LEDC of the solid-electrolyte interphase in lithium-ion batteries, Nano Energy 105 (2023) 107993. https://doi.org/10.1016/j.nanoen.2022.107993.

[188] F. Wang, G. Chen, N. Zhang, X. Liu, R. Ma, Engineering of carbon and other protective coating layers for stabilizing silicon anode materials, Carbon Energy 1 (2019) 219-245. https://doi.org/10.1002/ cey2.24.
[189] Y.Z. Li, J.M. Lu, Z.Y. Wang, X.Y. Wang, H.M. Yuan, N. Qin, Z.B. Yi, Z.H. Chen, S. Gu, Z.G. Lu, Suppressing continuous volume expansion of Si nanoparticles by an artificial solid electrolyte interphase for high-performance lithium-ion batteries, ACS Sustainable Chem. Eng. 9 (2021) 8059-8068. https://doi.org/10.1021/acssuschemeng.0c08964.
[190] F. Dou, Y.H. Weng, Q.Y. Wang, G.R. Chen, H.J. Liu, L.Y. Shi, D.S. Zhang, In situ imaging analysis of the inhibition effect of functional coating on the volume expansion of silicon anodes, Chem. Eng. J. 417 (2021) 128122. https://doi.org/10.1016/j.cej.2020.128122.
[191] H. Xie, C.P. Yang, Y.Y. Ren, S.M. Xu, T.R. Hamann, D.W. McOwen, E.D. Wachsman, L.B. Hu, Amorphous-carbon-coated 3D solid electrolyte for an electro-chemomechanically stable lithium metal anode in solid-state batteries, Nano Lett. 21 (2021) 6163-6170. https://doi.org/10.1021/acs. nanolett.1c01748.
[192] M. Yoon, Y.H. Dong, J. Hwang, J. Sung, H. Cha, K. Ahn, Y.M. Huang, S.J. Kang, J. Li, J. Cho, Reactive boride infusion stabilizes Ni-rich cathodes for lithium-ion batteries, Nat. Energy 6 (2021) 362-371. https://doi.org/10.1038/s41560-021-00782-0.
[193] M. Chen, F.M. Liu, S.S. Chen, Y.J. Zhao, Y. Sun, C.S. Li, Z.Y. Yuan, X. Qian, R. Wan, In situ self-catalyzed formation of carbon nanotube wrapped and amorphous nanocarbon shell coated $LiFePO_4$ microclew for high-power lithium ion batteries, Carbon 203 (2023) 661-670. https://doi.org/ 10.1016/j.carbon.2022.12.015.
[194] K.X. Wang, X.H. Li, J.S. Chen, Surface and interface engineering of electrode materials for lithium-ion batteries, Adv. Mater. 27 (2015) 527-545. https://doi.org/10.1002/adma.201402962.
[195] C.L. Jakobsen, B.P. Andersen, M. Johansen, C.K. Christensen, A.Ø. Drejer, M.A. Karlsen, D.B. Ravnsbæk, Structure and evolution of disordered deep-charge phases in Na_xCrO_2 Na-ion battery electrodes, J. Power Sources 591 (2024) 233875. https://doi.org/10.1016/j.jpowsour.2023.233875.
[196] Y.Z. Yue, Revealing the nature of glass by the hyperquenching-annealing-calorimetry approach, J. Non-Cryst. Solids: X 14 (2022) 100099.
[197] Y.F. Zhang, G. Yang, Y.Z. Yue, Calorimetric signature of structural heterogeneity in a ternary silicate glass, J. Am. Ceram. Soc. 96 (2013) 3035-3037.
[198] G. Jug, A. Loidl, H. Tanaka, On the structural heterogeneity of supercooled liquids and glasses, Europhys. Lett. 133 (2021) 56002.

Zhaoyang Wang is a lecturer at Liaocheng University. He received his Ph.D. Degree in Materials Science and Engineering from Wuhan University of Technology in 2020. His current research interests are mainly in electrode materials with disordered structures for lithium-ion batteries and sodium-ion batteries.

Zijuan Du obtained her B.S. degree from Wuhan University of Technology in 2016. She is currently a Ph.D. candidate in Materials Science and Engineering at Wuhan University of Technology. Her current research focuses on the preparation of disordered materials and their applications in electrochemical energy storage.

Luoqing Wang is an undergraduate student at Liaocheng University. He participated in Dr. Zhaoyang Wang's research group in October 2022. His current research interest is in amorphous cathode materials for lithium-ion batteries.

Guanjie He is an Associate Professor in Materials Chemistry at University College London (UCL). Prior to this position, he held faculty positions at QMUL, University of Lincoln. He has rapidly expanded his research activities, including through a growing number of collaborations in diverse areas from the core focus of aqueous energy storage and conversion materials and devices to advanced characterization and simulation.

Ivan P. Parkin is a Professor of Materials Chemistry, Dean of Faculty of Maths and Physical Sciences at University College London. He is a selected fellow of Royal Society of Chemistry and a member of Academia Europaea. His work focuses on the development of functional materials and thin films for energy storage application, photocatalysis, and wetting.

Yanfei Zhang received her Ph.D. degree in the Department of Physics from Shandong University, China, in 2009. From 2011 to 2012, she did her postdoc at Aalborg University, Denmark. She joined Qilu University of Technology as a lecturer in 2009 and currently is a Professor. Her research focuses on the glass electrode and electrolyte materials for lithium-ion batteries, glass relaxation and glass transition, structure and properties of oxide glasses and glass fibers.

Yuanzheng Yue is a Professor of Chemistry and Head of the Amorphous Functional Materials Group at Aalborg University, Denmark. He is a fellow of the European Academy of Sciences, the Royal Society of Chemistry, the European Ceramics Society, the Society of Glass Technology (UK), and a member of the Danish Academy of Natural Science. He is a council member of the International Commission on Glass (ICG) and chair of the ICG Technical Committee for Glass Fibers. His research focuses on glasses, glass fibers and disordered materials.